Forsythe N, Fowler HJ, Li XF, Blenkinsop S, Pritchard D.

Karakoram temperature and glacial melt driven by regional atmospheric circulation variability.

***Nature Climate Change* 2017,**

http://dx.doi.org/10.1038/NCLIMATE3361

Karakoram temperature and glacial melt driven by regional atmospheric circulation variability <for submission to Nature Climate Change>

Nathan Forsythe, Hayley J Fowler, Xiaofeng Li, Stephen Blenkinsop and David Pritchard

Affiliation (all authors) = Newcastle University, School of Civil Engineering & Geosciences

Summary

Identifying mechanisms driving spatially heterogeneous glacial mass-balance patterns in the Himalaya, including the "Karakoram anomaly", is crucial for understanding regional water resource trajectories. Streamflows dependent on glacial meltwater are strongly positively correlated with Karakoram summer air temperatures, which show recent anomalous cooling. We explain these temperature and streamflow anomalies through a circulation system – the Karakoram Vortex – identified using a regional circulation metric that quantifies the relative position and intensity of the westerly jet. Winter temperature responses to this metric are homogeneous across South Asia, but the Karakoram summer response diverges from the rest of the Himalaya. We show that this is due to seasonal contraction of the Karakoram Vortex through its interaction with the South-Asian monsoon. We conclude that interannual variability in the Karakoram Vortex, quantified by our circulation metric, explains the variability in energy-constrained ablation manifested in river flows across the Himalaya, with important implications for Himalayan glaciers' futures.

Background

The 'Karakoram Anomaly' was first identified by Hewitt[1] as a pattern of sub-regional positive glacial mass-balance. It has now been quantified by multiple glacial mass-balance studies[2,3,4,5,6,7,8] and is associated with cooling summer temperatures over the Karakoram[9]. This contrasts with patterns of warming temperatures and glacial retreat seen in other parts of the Himalaya. As elsewhere, the major controls on glacier mass-balance are snowfall accumulation and energy inputs (e.g. temperature, radiation) which drive ablation. Although streamflow seasonality in Indus tributaries is similar (Supplementary Figures 1B,D), there are characteristic hydrological regimes[10,11]. In high-elevation "glacial" catchments, annual streamflow is strongly controlled by summer energy inputs (Supplementary Figure 1C), with little correlation to winter precipitation amount (Supplementary Figure 1E). However, in middle-elevation "nival" catchments, streamflow is more strongly controlled by winter mass inputs (Supplementary Figure 1E). We present further information on climate and non-climatic influences on streamflow and glacier mass-balance in Indus tributaries in the Methods. As streamflows[13] from highly-glaciated Indus tributaries are declining, with implications for water resources of the densely-populated Indus Plains[13,14], it is unlikely that the Karakoram Anomaly is caused solely by recent increases in winter snowfall[15] offsetting increases in summer melt[16]. Here, we examine the role of regional-scale atmospheric circulation in controlling local climate across the sub-region and streamflow variability of Indus tributaries originating from the Karakoram. In glacial regime tributaries, streamflow variability provides an aggregate proxy of the ablation component of glacial mass-balance changes.

Cryospheric studies of the Third Pole Environment (TPE) and High Mountain Asia (HMA) have underlined the influence of atmospheric circulation on glacier mass-balance[17,18]. Previous studies have assessed the influence of large-scale atmospheric (-oceanic) modes, such as the North Atlantic Oscillation (NAO) and El Niño Southern Oscillation (ENSO), on HMA climate[19,20,21,22,23,24]. These

modes influence the mid-latitude Rossby wave train – a "circumglobal teleconnection"[24] – and allow atmospheric conditions in the North Atlantic and Pacific to influence the South Asian summer monsoon[19,23]. A positive NAO or warm-phase ENSO independently induce increased winter precipitation over the Western Himalaya[22], as westerly jet intensification causes more westerly disturbances[20,21]. Yet climate variability across the Himalayan arc cannot be explained through these teleconnections alone.

Identifying the Karakoram Zonal Index

Using methods described by Yadav[19,20], we tested the influence of a range of atmospheric circulation and surface variables from reanalyses on Karakoram locally station-observed 2m air temperature (T_{2m}) (stations detailed in Supplementary Table 1). We identified two areas of strong correlation, but opposing influence, for (westerly) zonal wind at 200-hPa and 500-hPa; pressure levels that roughly bound the westerly jet (see Methods). Figure 1A (inset) shows a "northern area" [40°N to 50°N, 52.5°E to 86.25°E], to the north of the Karakoram over Central Asia, between the Caspian Sea and Mongolia, while the "southern area" [20°N to 32.5°N, 52.5°E to 93.75°E] lies over the Indo-Gangetic Plains and northern Indian Ocean, from the Strait of Hormuz to the Bay of Bengal. Figure 1B shows the distinct annual cycle of zonal wind speed climatologies of the northern (Unorth) and southern (Usouth) areas at 200-hPa given by an ensemble of reanalyses (see Methods). Similar amplitude patterns, albeit with different absolute values, are found at 500-hPa. In the northern area, zonal wind speed is relatively constant throughout the year. In contrast, for winter months, when the westerly jet is positioned to the south of the Karakoram, the southern area displays high wind speeds. These decrease as monsoonal circulation develops through spring and summer and the the jet moves northward.

Other authors have investigated the influence of the westerly jet on western High Mountain Asia (HMA) climate[25,26], but examine only individual seasons (winter or summer) rather than the complete annual cycle. Our composite absolute metric, termed the "Karakoram Zonal Shear" (KZS), describes atmospheric conditions over the Karakoram by differencing the areal mean monthly zonal wind speed (U) for the northern minus the southern region (Figure 1B). The KZS is a variation of the general "Zonal Index"[27], but geographically focused on the Karakoram and expressed in units of velocity rather than pressure. It has a similar longitudinal range to the Webster and Yang Monsoon Index (WYMI)[28] but uses horizontal rather than vertical shear. The KZS northern influence area also overlaps the northern half of the domain used for the middle-upper troposphere temperature index (MUTTI)[26]. Neither the WYMI nor the MUTTI, however, were designed to capture circulation influences on the Karakoram or to quantify circulation through the complete annual cycle.

In meteorological terms, the KZS is the north-south shear of zonal wind, denoting the latitudinal position and change in intensity of the westerly jet upstream of the Karakoram. It has a sinusoidal annual cycle that is strongly negative during the boreal winter and strongly positive during peak monsoonal activity (Figure 1B). We next produce a relative metric, termed the "Karakoram Zonal Index" (KZI), by standardising the KZS (subtracting period mean and then dividing by period standard deviation). As a dimensionless seasonal aggregation of either winter (JFM) or summer (JJA) circulation conditions, the KZI enables us to work in 'anomaly space' to investigate atmospheric linkages with local climate. A positive (negative) KZI state indicates an anomalous northward (southward) shift in the 'intensity-position' moment of the westerly jet relative to the climatological mean.

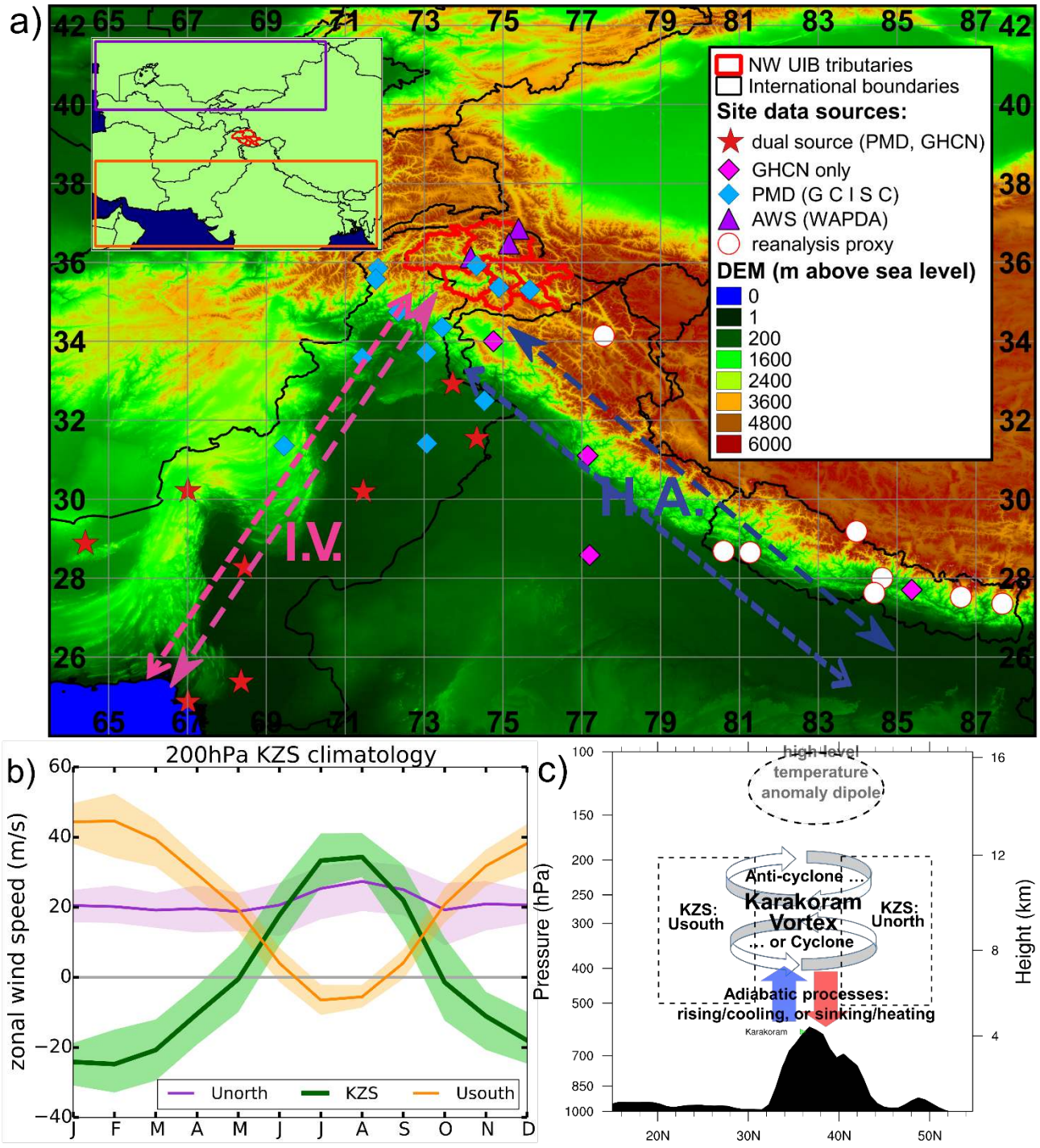

[Figure 1] Geographic definition, resulting zonal wind climatologies and conceptual structures for the Karakoram Zonal Shear (KZS). A) Locations and data origin for T_{2m} station observations used. B) 200-hPa reanalysis-ensemble climatology (lines = mean, shaded area = 10^{th} to 90^{th} percentiles range) of zonal wind speeds in the northern (Unorth, in purple) and southern (Usouth, in orange) areas, and the KZS (in green), i.e. north minus south. C) a cross-section conceptual diagram of the KZS in relation to atmospheric processes and structures. In A) T_{2m} station transects are shown as "I.V." (Indus Valley, latitudinal) and "H.A." (Himalayan Arc, longitudinal).

A circulation system driving KZI-T_{2m} response

To explore atmospheric processes underlying the spatial patterns of the KZI-T_{2m} response, we correlate KZI with T_{2m} from ERA-Interim (1979-2010) and overlay period-mean 500-hPa (near-surface of Tibetan Plateau) horizontal wind streamlines resolved from zonal (U) and meridional (V) components (Figure 2). Areas of positive (negative) correlation between KZI and T_{2m} correspond to anticyclonic (cyclonic) anomalies in both winter (JFM) and summer (JJA). Winter correlations between the KZI and T_{2m} are almost uniformly positive across HMA (Figure 2A). This contrasts with summer, where positive correlations are restricted to the Karakoram and western tail of the Tibetan Plateau, while negative correlations cover the Indo-Gangetic Plains (Figure 2B). These seasonal spatial patterns are confirmed through alternate visualisations both as aggregates of top and bottom quartile KZI cases (Supplementary Figure 2) and maximum and minimum KZI years (Supplementary Figure 3).

Physically, the KZI reveals a "Warm High/Cold Low" response of T_{2m} to (anticyclonic/cyclonic) circulation state throughout the year, characterised by a persistent anomalous regional vortex system we designate the "Karakoram Vortex" (KV). The KV, and its relationship to the KZS influence areas and relevant atmospheric processes, is shown in Figure 1C.

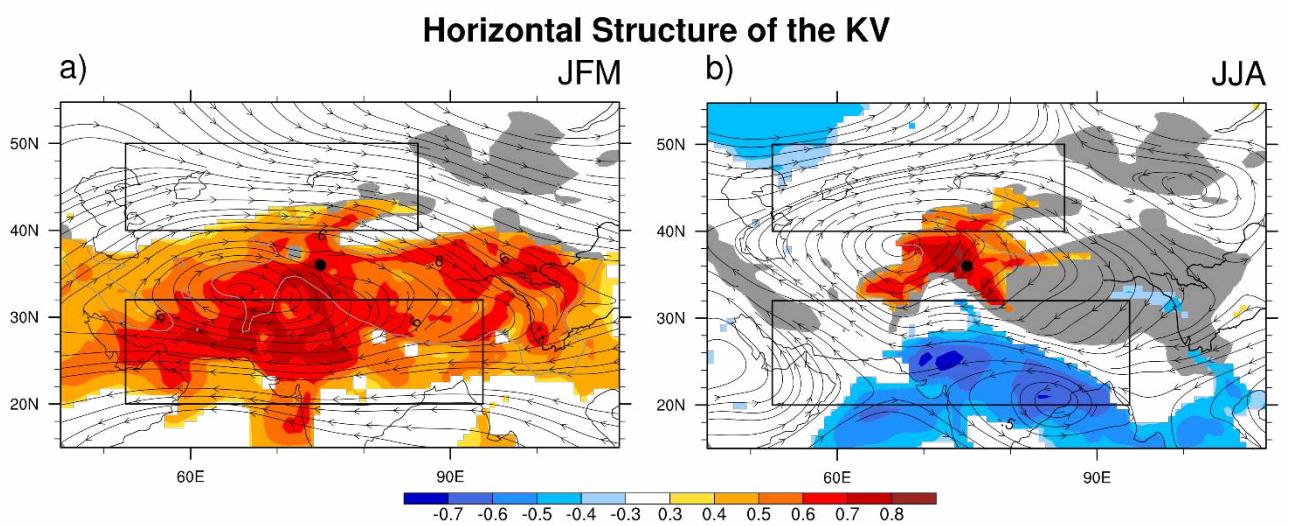

[Figure 2] Pearson correlations (colour-shaded) between KZI and T_{2m} from ERA-Interim for 1979-2010 for a) winter (JFM), and b) summer (JJA), reveal the Karakoram Vortex (KV). Streamlines show the resolved 500-hPa horizontal wind (U,V) as period mean. Colour-shading denotes significant correlations above the 0.05 level. The black boxes denote northern and southern KZI influence areas (same as Fig. 1A). Black dot denotes the central position (36°N, 75°E) of Karakoram focus area. Grey-shading denotes topography above 1,500 m.

The KV is an anomalous deep vortex circulation system which develops within the dominant westerlies, spanning from the near-surface of the Western Tibetan Plateau to near the tropopause. By seasonally compositing air temperature and wind anomalies perpendicular (meridional/V, vertical/W) to a north-south transect centred on the Karakoram (70°E to 80°E) during strongly positive and negative KZI conditions, we show the superposition of strong temperature anomalies with strong vertical wind anomalies in the central column of the KV (Figure 3). In winter, strongly positive (negative) KZI conditions yield warm (cool) surface-level air temperature anomalies between 20°N and 45°N. These air temperature anomalies extend upward through the troposphere, reaching 300-

hPa or more over the southern face of the central Karakoram. During positive (negative) KZI conditions, vertical circulation anomalies in areas with the largest warmer (cooler) temperature deviations are strongly downward (upward), i.e. the anomalous atmospheric mass penetrates downward (upward) into the denser (lighter) pressure levels with an anomalous volume compression (expansion), suggesting substantial adiabatic influence. In summer, the latitudinal range of coherent T_{2m} anomalies shrinks considerably but remains centred on the Karakoram. Here, the temperature anomalies extend upward in a column to 200-hPa before deflecting horizontally northward: these warm (cool) anomaly 'plumes' correspond to strong downward (upward) vertical wind anomalies, again pointing to adiabatic effects. Our results are consistent with Zhao et al.[26] who demonstrate that a summer ascending motion is linked to a southward shift of the jet (a negative KZI). Yadav[29] also identified adiabatic processes associated with the mid-latitude wave train when analysing an atmospheric column over Iran, to the west of our study area. For all seasons and KZI phase combinations there is a dipole over the Karakoram between air temperature anomalies from the surface to ~250-hPa and the stratosphere above. Exploration of the mechanisms involved in this dipole, however, is beyond the scope of the present work.

We thus find that as the westerly jet intensifies northward (southward), KZI becomes progressively more positive (negative). This produces increasingly anticyclonic (cyclonic) conditions over the central Karakoram. In winter, these conditions extend homogenously across the entire region. In summer, however, under positive (negative) KZI conditions anomalous anti-cyclonic (cyclonic) circulation is tightly focused on the Karakoram, with concurrent cyclonic (anti-cyclonic) activity affecting the Indo-Gangetic Plain. We further find the Karakoram T_{2m} observations have a higher correlation with the KZI (see Methods) than with other large-scale circulation modes (Supplementary Information), such as the NAO or ENSO, and for the WYMI[28] (see Supplementary Figure 4). Linear regression indicates that one positive (negative) standard deviation of KZI yields a Karakoram T_{2m} increase (decrease) of 0.59°C (+/-0.19°C, R^2=0.32, p=0.005) in winter and 0.74°C (+/-0.14°C, R^2=0.57, p<0.001) in summer. Similarly, summer streamflow from the "glacial-regime" Hunza tributary of the Indus increases (decreases) by 13.6% (+/-2.4%, R^2=0.405, p<0.001) for one positive (negative) standard deviation of KZI. This shows the sensitivity of "glacial" tributary streamflows[16,30] to the KZI through its effects on summer temperatures, which has substantial downstream implications[13] for irrigated agriculture and hydropower generation.

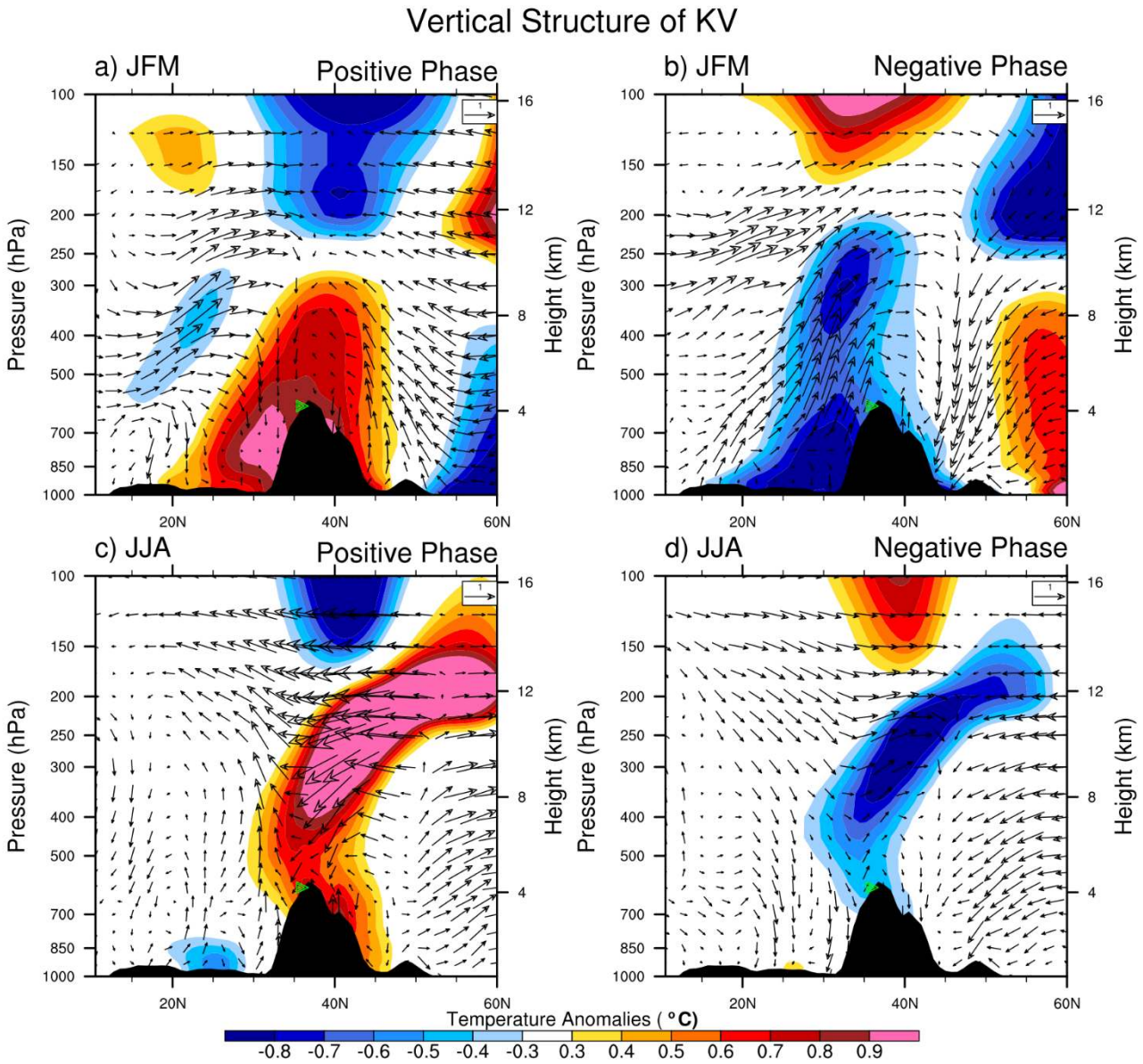

[Figure 3] Transect of composite air temperature (colour shading) and (V,W) wind anomalies (vectors) for positive (A,C) and negative (B,C) KZI conditions in winter (JFM: A,B) and summer (JJA: C,D) from ERA-Interim for 1979-2010. Positive (negative) phase compositing is for KZI greater (less) than plus (minus) 0.55 (standard deviations). This yields the upper (lower) quartiles, i.e. >75th (<25th) percentile. Representative (anomaly) vector length scale is shown in the upper right corner of each panel. This transects is an integration from 70°E to 80°E. The green triangle denotes the central Karakoram (36°N, 75°E).

Temporal variability of KZI and Karakoram T_{2m}

The KZI quantifies regional atmospheric conditions. Its inter-annual variability is high, with frequent sign changes in both winter and summer (Figure 4A,B). We demonstrate – through striking synchronisation between KZI and observations of T_{2m} at both valley (PMD T_{2m} in Figure 4A,B) and high-elevation automatic weather stations (AWS T_{2m} in Figure 4A,B) – that the atmospheric circulation conditions described by the KZI can explain a large fraction of T_{2m} interannual variability. For summer, the correlation between KZI and PMD T_{2m} time-series for 1961-2010 yields a Mann-Kendall tau (τ) of 0.585 ($p<0.0001$). In contrast, the relative weakness of the winter relationship

(τ=0.283, p=0.0037) suggests that processes not directly linked to the KZI, including cloud-cover[31], may play a larger role in governing Karakoram cold-season T_{2m} variability. We find significant trends (p<0.05) for both winter (τ=0.198, p=0.042) and summer (τ=-0.218, p=0.026) Karakoram $T_{2m,}$ as well as summer KZI (τ=-0.224, p=0.021), but not for winter KZI (τ=0.007, p=0.940). This suggests that atmospheric circulation variability has a larger causal role in temperature change in summer than for winter over recent decades. An intensification and northward shift in the winter-time westerly jet over western HMA between 1979 and 2011[25] is consistent with the behaviour of the winter KZI (Figure 4A) and its northern component (Figure 4C), specifically with more negative anomalies from 1980 to 1990 and frequent positive anomalies after 2000. The trend in winter T_{2m} is positive indicating warming, while trends in both summer KZI and summer T_{2m} are negative, indicating cooling over the Karakoram and relative southward displacement of the westerly jet intensity during key months for glacial-melt over 1960-2010.

Our demonstrated links between the KZI and T_{2m}, and established links between T_{2m} and streamflow for "glacial-regime" Indus tributaries[16,30], suggest that such streamflow should be responsive to KZI. Figure 4E shows Kendall Tau correlations between KZI and summer streamflow in Indus tributaries with respect to catchment glaciated fraction. The near linear relation equates to a spectrum of hydrological regimes, i.e. glacial to nival (see Methods). Summer streamflow for glacial regime tributaries show strong positive correlations to KZI, e.g. for Hunza, τ=0.440 (p<0.0001). Nival and mixed regime catchments have near null and weak/moderate positive correlations respectively. We compare summer streamflow anomalies against KZI for the most glaciated Indus tributary, the Hunza, in Figure 4F. The strong similarities between Figures 4B and 4F further illustrate the influence of KZI on Indus tributary flows via T_{2m} as a component of energy which drives ablation and meltwater generation.

As the south flank of the KV is coupled with the South Asia summer monsoon (SASM) flow, the negative tendency of the KV is consistent with a weakening of the South Asian summer monsoon[32,33,34] and it is in good correspondence with the WYMI (Figure 4B and Supplementary Figure 4). Anomaly time-series for Unorth and Usouth KZI components (Figure 4C,D) show an essentially uniform distribution of positive and negative anomalies for both in winter, and for Unorth in summer. However, Usouth shows strong negative anomalies (<-2.0) in summer prior to 1985; after this anomalies become progressively less negative. Physically, this corresponds to a weakening of normally easterly winds in peak monsoon months (Figure 1B), supporting previous studies showing a weakening of Indian monsoonal circulation[32,33,34], but contrasting with the relatively stable behaviour of the westerly jet over Central Asia (Unorth, Figure 4D).

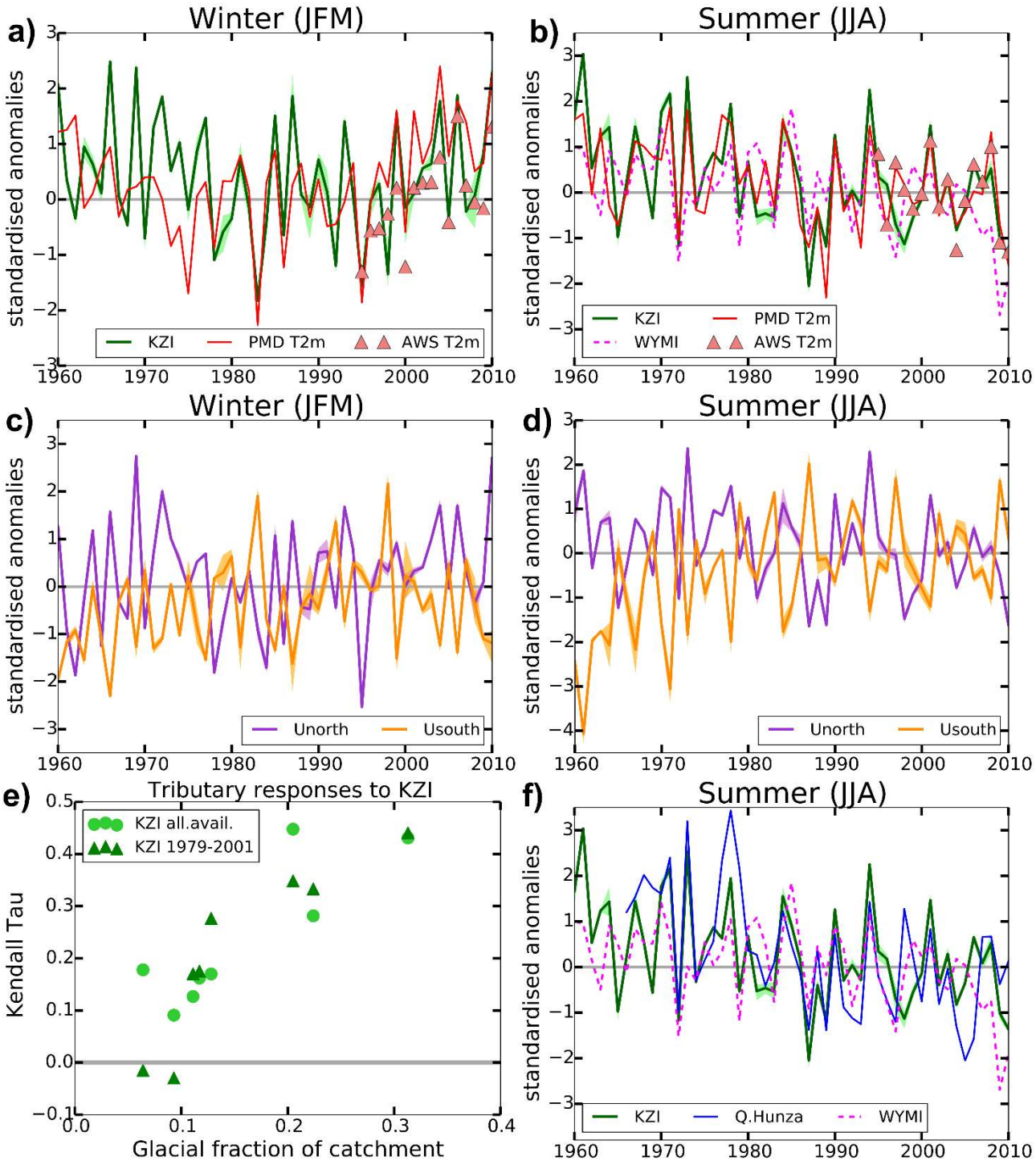

[Figure 4] KZI influence on Karakoram T_{2m} and Indus tributary streamflows. A) winter (JFM) and B) summer (JJA) time-series of standardised anomalies of KZI estimates and Karakoram local T_{2m} observations. Unorth and Usouth (components of KZI) time-series are shown in C (winter) and D (summer). KZI influence on Indus tributary summer streamflows is shown as: E) Kendall Tau correlation between concurrent KZI and streamflow with respect to fractional glaciated area; and F) time-series of KZI and streamflow from the Hunza catchment (Q. Hunza). Stations incorporated in time-series in A and B are PMD T_{2m} and AWS T_{2m} from Figure 1A. In A to D, ensemble spread for KZI, Unorth and Usouth are shown with shading. In B and F (summer) the Webster and Young Monsoon Index (WYMI) is plotted in addition to KZI. Catchment boundaries and gauging locations of selected Indus tributaries are shown in Supplementary Figure 1.

Sub-regional differences in KZI-T_{2m} response

We now examine sub-regional differences in T_{2m} response to the KZI to explore why temperature influence on glacial mass-balance in the Karakoram diverges from conditions elsewhere in HMA. Specifically, we compare correlation patterns between the KZI and T_{2m} observations for three transects (Figure 5): vertically within the NW UIB, (Figure 5A), longitudinally across the 'Himalayan Arc' (Figure 5B), and latitudinally along the 'Indus Valley' (Figure 5C). Some points along the longitudinal transect were substituted with T_{2m} proxies from reanalyses (Figure 1A, Methods). In these transects Kendall tau correlation coefficients with the KZI reach magnitudes as high as 0.6.

We find no discernible signal in the vertical transect (Figure 5A), suggesting that KZI influence is not modulated by elevation-dependent processes. In contrast, there is a clear shift away from strongly positive correlations in summer as one moves eastward from 76°E, and southward from 34°N. Longitudinally (Figure 5B), there is a severe discontinuity at the meridian linking Leh, Shimla and New Delhi (~77°E); summer T_{2m} in Ladakh (Leh) shows strong positive correlation with KZI, but stations in the Central Himalaya (Shimla) and the Gangetic plain (New Delhi) show strong negative correlations. Moving eastward, summer correlations become progressively less negative until they are weakly positive again in eastern Nepal. Latitudinally (Figure 5C), moving south from the Karakoram in the Indus Valley, positive correlations in summer decrease progressively until they are strongly negative near to the Arabian Sea.

Sub-regional differences in strength and sign of correlations between summer KZI and T_{2m} contrast starkly with uniformly strong positive correlations in winter across HMA and South Asia. From this we conclude that changes in cold-season atmospheric circulation regime, as quantified by the KZI, would have broadly homogenous regional effects. However, changes to atmospheric circulation during peak melt-season would have the opposite effect on Karakoram T_{2m} compared with the Central Himalaya, with contrasting effects on meltwater volumes and glacial mass-balance for the Indus and Ganges basins.

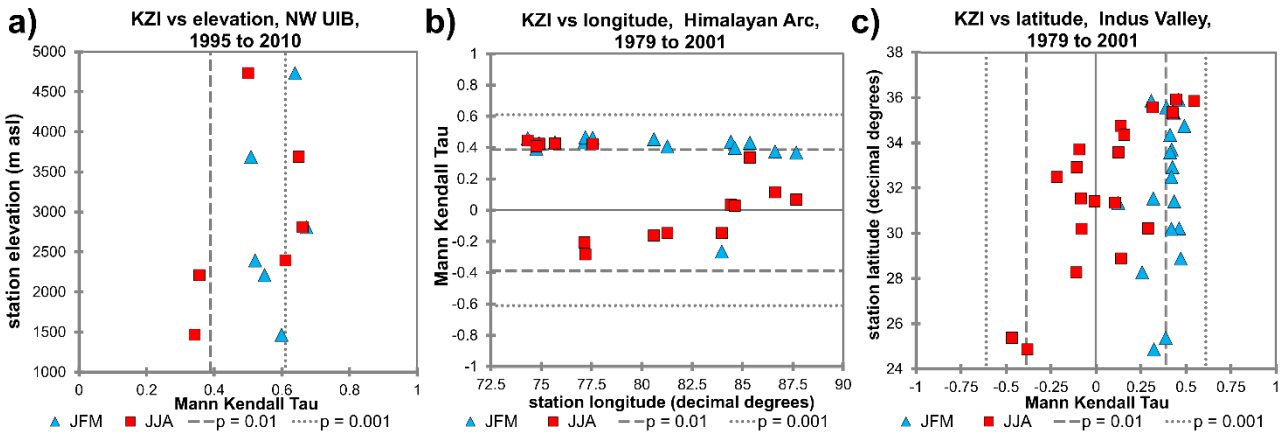

[Figure 5] Seasonal correlations between KZI and local T_{2m} observations along transects: A) vertical, 1500m to 4500m a.s.l., 1995-2010, B) longitudinal, ~74°E to 87.5°E, 1979-2001, and C) latitudinal, ~25°N to 36°N,1979-2001, transects. Stations are shown in Figure 1A: A) vertical transect stations within the NW UIB (red boundaries); time-period differs as AWS records are only available from 1995; B) Himalayan arc transect stations along the blue dashed line (H.A.); C) Indus Valley transect stations along the magenta dashed line (I.V.).

Discussion

We have defined a new composite metric that describes atmospheric conditions over the Karakoram region, the Karakoram Zonal Shear (KZS). The KZS has a strong annual cycle, quantifying the coupled strength and position of the westerly jet over western HMA. Its standardised form is a dimensionless metric, the Karakoram Zonal Index (KZI), and quantifies the northward (southward) shift of this 'intensity-position' moment as positive (negative) values. Using these metrics, we have identified an anomalous circulation system that influences T_{2m} over HMA, the Karakoram Vortex (KV). In winter, KV anomalies extend broadly across South Asia, with warm (cool) responses to anti-cyclonic (cyclonic) regional circulation conditions. However, in summer the KV's southern branch is coupled with the Indian Monsoon; thereby, the KZI can be interpreted as the interplay between the westerly jet and the South Asian monsoon[35] and is correlated to the WYMI. This corroborates previous work by Zhao et al.[26] who linked strong cold air advection into western HMA in summer with weak monsoonal circulation development.

We have further presented strong evidence that declining flows in highly-glaciated Indus tributaries[12] and recent summer cooling of T_{2m}[9] over the Karakoram – likely contributors to the 'Karakoram anomaly' of glacial mass-balance stability – are due, at least in part, to large-scale atmospheric circulation conditions in the form of the latitudinal position (of maximum intensity) of the westerly jet west of HMA. We have shown that the driving mechanisms for summer cooling over the Karakoram include adiabatic cooling associated with strong vertical circulations during negative summer KZI events. In these cases cyclonic conditions dominate the Karakoram with an increased passage of westerly depressions and corresponding increased cloud cover and decreased insolation. It is beyond the scope of this paper to determine whether the recent decreasing tendency in summer KZI – quantifying a more southerly jet position and peak intensity in summer – is likely to continue. Indeed, a global analysis of historical trends in jet streams found general poleward migration in the Northern Hemisphere, while noting that local and seasonal trends may differ[36]. To develop a fully comprehensive characterisation of HMA and South Asia regional climate behaviour, it will be necessary to identify interactions between the dynamical features we describe (KZI, KV) and thermal forcings[37] over the Tibetan Plateau and Bay of Bengal.

Independent of KZI trend, it is an open question whether atmospheric conditions described by the KZI will continue to dominate Karakoram T_{2m} anomalies or simply modulate short-term variability in a context overwhelmed by background global warming. We conclude that atmospheric circulation dynamics– quantified by the KZI – have an important influence on glacial ablation through T_{2m} and result in contrasting glacial mass-balance patterns across the Himalaya. Therefore, accurate representation of the KZI-T_{2m} relationship in climate models is essential for robust assessment of potentially divergent climate change impacts on Himalayan rivers and the glaciers which feed them.

REFERENCES

[1] Hewitt, K., 2005. The Karakoram Anomaly? Glacier Expansion and the 'Elevation Effect,' Karakoram Himalaya. *Mountain Research and Development*, **25** (4), 332-340. http://dx.doi.org/10.1659/0276-4741(2005)025[0332:TKAGEA]2.0.CO;2

[2] Bolch, T., Kulkarni, A., Kääb, A., Huggel, C., Paul, F., Cogley, J. G., Frey, H., Kargel, J. S., Fujita, K., Scheel, M., Bajracharya, S. and Stoffel, M., 2012. The State and Fate of Himalayan Glaciers. *Science*, **336** (6079), 310-314. http://dx.doi.org/10.1126/science.1215828

[3] Kääb, A., Berthier, E., Nuth, C., Gardelle, J., and Arnaud, Y., 2012. Contrasting patterns of early twenty-first-century glacier mass change in the Himalayas. *Nature* **488** (7412), 495-498. http://dx.doi.org/10.1038/nature11324

[4] Gardelle, J., Berthier, E. and Arnaud, Y., 2012. Contrasting patterns of early twenty-first-century glacier mass change in the Himalayas. *Nature Geosci*. **5** (5), 322-325. http://dx.doi.org/10.1038/ngeo1450

[5] Jacob, T., Wahr, J., Pfeffer, T. W. and Swenson, S., 2012. Recent contributions of glaciers and ice caps to sea level rise. *Nature* **482**, 514–518. (http://dx.doi.org/10.1038/nature10847).

[6] Pratap, B., Dobhal, D.P., Bhambri, R., Mehta, M., Tewari, V.C., 2016. Four decades of glacier mass balance observations in the Indian Himalaya. *Regional Environmental Change*, **16** (3), 643-658. DOI: 10.1007/s10113-015-0791-4

[7] Bolch, T., Pieczonka, T., Mukherjee, K. and Shea, J., 2017. Brief communication: Glaciers in the Hunza catchment (Karakoram) have been nearly in balance since the 1970s. *The Cryosphere*, **11**, 531–539. http://dx.doi.org/10.5194/tc-11-531-2017

[8] Zhou, Y., Li, Z., and Li, J. I., 2017. Slight glacier mass loss in the Karakoram region during the 1970s to 2000 revealed by KH-9 images and SRTM DEM. *J. Glaciol.*, **63** (238), 331-342 http://dx.doi.org/10.1017/jog.2016.142.

[9] Fowler, H. J. and Archer, D. R., 2006. Conflicting Signals of Climate Change in the Upper Indus Basin, *J. Climate*, **19** (17), 4276–4292. http://dx.doi.org/10.1175/JCLI3860.1

[10] Archer, D. R., 2003. Contrasting hydrological regimes in the Indus Basin. *J. Hydrol*., **274** (1-4), 198–210. http://dx.doi.org/10.1016/S0022-1694(02)00414-6

[11] Forsythe, N., Fowler, H.J., Kilsby, C.G. and Archer, D.R., 2012a. Opportunities from remote sensing for supporting water resources management in village/valley scale catchments in the Upper Indus Basin. *Water Resources Management*, **26** (4), 845–871. http://dx.doi.org/10.1007/s11269-011-9933-8

[12] Sharif, M., Archer, D. R., Fowler, H. J. and Forsythe, N., 2013. Trends in timing and magnitude of flow in the Upper Indus Basin. *Hydrol. Earth Syst. Sci.*, **17** (4), 1503-1516. http://dx.doi.org/10.5194/hess-17-1503-2013

[13] Archer, D.R, Forsythe, N., Fowler, H.J. and Shah, S.M., 2010. Sustainability of water resources management in the Indus Basin under changing climatic and socio economic conditions. *Hydrol Earth Syst Sci* **14**, 1669–1680. http://dx.doi.org/10.5194/hess-14-1669-2010

[14] Immerzeel, W.W., Van Beek, L.P.H. and Bierkens, M.F.P., 2010. Climate change will affect the Asian water towers. *Science*, **328** (5984), 1382–1385. http://dx.doi.org/10.1126/science.1183188

[15] Archer, D. R. and Fowler, H. J., 2004. Spatial and temporal variations in precipitation in the Upper Indus Basin, global teleconnections and hydrological implications. *Hydrol. Earth Syst. Sci.*, **8** (1), 47–61. http://dx.doi.org/10.5194/hess-8-47-2004

[16] Forsythe, N., Kilsby, C.G., Fowler, H.J. and Archer, D.R., 2012. Assessment of Runoff Sensitivity in the Upper Indus Basin to Interannual Climate Variability and Potential Change Using MODIS Satellite Data Products. *Mountain Research and Development*, **32** (1), 16-29. http://dx.doi.org/10.1659/MRD-JOURNAL-D-11-00027.1

[17] Yao, T., Thompson, L., Yang, W., Yu, W., Gao, Y., Guo, X., Yang, X., Duan, K., Zhao, H., Xu, B., Pu, J., Lu, A., Xiang, Y., Kattel, D.B. and Joswiak, D., 2012. Different glacier status with atmospheric circulations in Tibetan Plateau and surroundings. *Nature Climate Change*, **2** (9), 663-667. http://dx.doi.org/10.1038/nclimate1580

[18] Mölg, T., Maussion, F. and Scherer, D., 2014. Mid-latitude westerlies as a driver of glacier variability in monsoonal High Asia. *Nature Climate Change*, **4** (1), 68-73. http://dx.doi.org/10.1038/nclimate2055

[19] Yadav, R.K., 2009. Changes in the large-scale features associated with the Indian summer monsoon in the recent decades. *International Journal of Climatology*, **29** (1), 117-133. DOI: 10.1002/joc.1698

[20] Yadav, R.K., Rupa Kumar, K. and Rajeevan, M., 2009. Increasing influence of ENSO and decreasing influence of AO/NAO in the recent decades over northwest India winter precipitation. *Journal of Geophysical Research: Atmospheres*, **114** (12), art. no. D12112. http://dx.doi.org/10.1029/2008JD011318

[21] Yadav, R.K., Ramu, D.A., Dimri, A.P. 2013. On the relationship between ENSO patterns and winter precipitation over North and Central India. *Global and Planetary Change*, **107**, 50-58. DOI: 10.1016/j.gloplacha.2013.04.006

[22] Syed, F.S., Giorgi, F., Pal, J.S. and King, M.P., 2006. Effect of remote forcings on the winter precipitation of central southwest Asia part 1: observations, *Theor. Applied Climatology* **86**: 147–160. http://dx.doi.org/10.1007/s00704-005-0217-1

[23] Ding, Q., Wang, B., Wallace, J.M. and Branstator, G., 2011. Tropical-extratropical teleconnections in boreal summer: Observed interannual variability. *Journal of Climate*, **24** (7), 1878-1896. http://dx.doi.org/10.1175/2011JCLI3621.1

[24] Ding, Q. and Wang, B., 2005. Circumglobal teleconnection in the Northern Hemisphere summer. *Journal of Climate*, **18** (17), 3483-3505. http://dx.doi.org/10.1175/JCLI3473.1

[25] Cannon, F., Carvalho, L.M.V., Jones, C., Bookhagen, B., 2014. Multi-annual variations in winter westerly disturbance activity affecting the Himalaya. *Climate Dynamics*, **44** (1-2), 441-455. http://dx.doi.org/10.1007/s00382-014-2248-8

[26] Zhao, Y., Huang, A., Zhou, Y., Huang, D., Yang, Q., Ma, Y., Li, M. and Wei, G., 2014. Impact of the middle and upper tropospheric cooling over central Asia on the summer rainfall in the Tarim Basin, China. *Journal of Climate*, **27** (12), 4721-4732. http://dx.doi.org/10.1175/JCLI-D-13-00456.1

[27] Oliver, J.E. "Zonal Index" (entry in) *Encyclopedia of World Climatology*, 820-822. DOI:10.1007/1-4020-3266-8_229

[28] Webster, P.J. and Yang, S., 1992. Monsoon and ENSO: selectively interactive systems. *Quarterly Journal - Royal Meteorological Society*, **118** (507), 877-926. http://dx.doi.org/10.1002/qj.49711850705

[29] Yadav, R.K., 2016. On the relationship between Iran surface temperature and northwest India summer monsoon rainfall. *International Journal of Climatology*, **36**, 4425-4438. DOI: 10.1002/joc.4648

[30] Archer, D. R., 2004. Hydrological implications of spatial and altitudinal variation in temperature in the Upper Indus Basin. *Nord. Hydrol*, **35** (3), 209–222.

[31] Forsythe, N., Hardy, A.J., Fowler, H.J. Blenkinsop, S., Kilsby, C.G., Archer, D.R. and Hashmi, M.Z., 2015. A detailed cloud fraction climatology of the Upper Indus Basin and its implications for near surface air temperature. *Journal of Climate*, **28** (9), 3537-3556. DOI:10.1175/JCLI-D-14-00505.1

[32] Dash, S.K., Kulkarni, M.A., Mohanty, U.C. and Prasad, K., 2009. Changes in the characteristics of rain events in India. *Journal of Geophysical Research: Atmospheres*, **114** (10), art. no. D10109. http://dx.doi.org/10.1029/2008JD010572

[33] Bollasina, M.A., Ming, Y. and Ramaswamy, V., 2011. Anthropogenic aerosols and the weakening of the south asian summer monsoon. *Science*, **334** (6055), 502-505. http://dx.doi.org/10.1126/science.1204994

[34] Saha, A., Ghosh, S., Sahana, A.S., Rao, E.P., 2014. Failure of CMIP5 climate models in simulating post-1950 decreasing trend of Indian monsoon. *Geophysical Research Letters*, **41** (20), 7323-7330. http://dx.doi.org/10.1002 /2014GL061573

[35] Saeed, F., Hagemann, S. and Jacob, D., 2012. A framework for the evaluation of the South Asian summer monsoon in a regional climate model applied to REMO. *International Journal of Climatology*, **32** (3), pp. 430-440. http://dx.doi.org/10.1002/joc.2285

[36] Archer, C.L. and Caldeira, K., 2008. Historical trends in the jet streams. *Geophysical Research Letters*, **35** (8), art. no. L08803. http://dx.doi.org/10.1029/2008GL033614

[37] Wu, G., Duan, A., Liu, Y., Mao, J., Ren, R., Bao, Q., He, B., Liu, B., and Hu, W., 2015. Tibetan Plateau climate dynamics: recent research progress and outlook. *National Science Review*, **2**, 100–116. doi: 10.1093/nsr/nwu045

Acknowledgements

Karakoram T_{2m} observations were obtained both directly from the Pakistan Meteorological Department and via the Global Change Impacts Studies Centre (Islamabad). Upper Indus tributary streamflow observations were obtained, via intermediaries including Mr Daniyal Hashmi, from the Pakistan Water and Power Development Authority. This study was made possible by financial support from the Leverhulme Trust via a Philip Leverhulme Prize (2011) awarded to H.F. Additional financial support during the developmental stages of this work was provided by the British Council Pakistan (PMI2/RCPK06 and INSPIRE/SP0015 grants), the UK Natural Environment Research Council (NERC) as a Postdoctoral Fellowship award NE/D009588/1 (2006–2010) to H.F., and a U.S. National Science Foundation (NSF) Graduate Research Fellowship (ID:2006037346) award to N.F. (2006–2010). H.F. is supported by a Royal Society Wolfson Research Merit Award (WM140025). X.L., S.B. and H.F. are supported by the INTENSE project through the European Research Council (grant ERC-2013-CoG-617329).

Author contributions: N.F. designed the study, processed and analysed the data, created most of the figures (1, 4, 5 and all Supplementary except Figure 4), and wrote the paper. All other co-authors wrote and edited the paper and assisted in interpretations. H.F. provided overall leadership, interpretation and integration of results and methodological guidance. S.B. focused on readability for the broader Nature Climate Change audience and methodological guidance. X.L. provided input on climatological mechanisms and created Figures 2, 3 and Supplementary Figure 4. D.P. provided input on recent variability of Indus tributary streamflows.

Author Information: Reprints and permissions information is available at www.nature.com/reprints. The authors declare no competing financial interests. Readers are welcome to comment on the online version of this article at www.nature.com/nature. Correspondence and requests for materials should be addressed to N.F. (nathan.forsythe@ncl.ac.uk).

METHODS

Hydrological regimes of the Upper Indus tributaries

For those readers unfamiliar with the body of literature[10,11,12,13,15,16,30] explaining hydrological regimes of the Upper Indus basin, we provide here a brief primer. While it is a cliché to refer to the glaciated areas of High Mountain Asia as the "third pole" and high-elevation tributary catchments which drain them as "water towers for the continent", there is a strong earth science basis for these terms. The frozen water stored in the glaciers of HMA constitutes a vast reservoir to potentially buffer interannual variability in precipitation, provided that sufficient energy inputs (T_{2m}) are available to drive meltwater generation and thus supply streamflow to downstream areas. Upper Indus tributaries are far from homogeneous in their degree of glaciation (Supplementary Figure 1A). Nevertheless, the vast majority of annual precipitation across the Upper Indus falls as snow. In catchments with substantial glacial cover, and in particular with large ice volumes at elevations low enough to experience summer melting, available (solid) water mass is in surplus, and energy inputs (T_{2m}) become the limiting factor controlling streamflow generation. Such catchments are considered to have a "glacial" hydrological regime. In contrast, the variability of streamflow in catchments with scant glaciation is predominantly governed by mass inputs (cold season snow accumulation) as there is more energy (T_{2m}) available during summer than necessary to achieve complete ablation. These are denoted as "nival" regime catchments. Unsurprisingly, areas with moderate glaciation respond (hydrologically) to both interannual variability in winter precipitation and summer energy inputs (T_{2m}) and are thus classified as "mixed" regime. In terms of seasonality of river flows, however, because the high-elevation catchments of all three regimes experience relatively cold winters, conditions (e.g. 0°C isotherm elevations) are only conducive to meltwater generation from late spring through early autumn (April to October). Thus the hydrological regime can in practice be difficult to identify solely from the annual catchment hydrograph, as is illustrated in the similarities between two example catchments in Supplementary Figure 1: "glacial" regime, Hunza (Supplementary Figure 1B) and "nival" regime, Astore (Supplementary Figure 1D). Comparison of the strength of correlations between climate forcings and streamflow, on the other hand, does reveal the catchment hydrological regime. Energy inputs (indexed by T_{2m}, Supplementary Figure 1C) have a near null or weak negative correlation with summer streamflow from nival regime (low glacial fraction) catchments. Nival regime catchments' streamflows instead responds to mass inputs (Supplementary Figure 1E), with strong positive correlation to winter precipitation but near null correlation to summer (melt-concurrent) precipitation. Glacial regime (high glacial-fraction) catchments show strong positive correlations to energy inputs (Supplementary Figure 1C) but only weak or negative correlation to mass inputs (Supplementary Figure 1E), specifically a near null correlation to winter precipitation and weak/moderate negative correlation to summer precipitation. This negative correlation between summer streamflow and concurrent precipitation in glacial regime catchments occurs because climate conditions are often simultaneously cold and wet or warm and dry. Physical mechanisms for this anti-correlation include the reduction of incoming shortwave radiation due to increased cloud cover during cyclonic weather, and a reduction of net shortwave radiation to melt surfaces through "whitening" (increased albedo) due to fresh snowfall.

As a point of clarification on the indicators of energy inputs quantified by near surface air temperature, in Supplementary Figure 1C we consider the monthly means of daily average (Tavg) and daily minimum (Tmin), from both local observations (suffix ".obs") and an ensemble of global meteorological reanalyses (suffix ".rean"), having first transformed all indicators into "anomaly space" through standardisation. We present correlation results for both Tavg and Tmin because Tavg

is very frequently used for temperature index ("degree-day") methods of snowmelt modelling, while Tmin has been shown previously[16,30] to provide a marginally stronger predictor of river discharge from highly glaciated basins. The physical basis for this is thought to be a sensitivity of intra-glacier meltwater generation and meltwater routing due to thermal inertia, i.e. diurnal refreezing when Tavg is >0°C but Tmin < 0°C.

As a result of the strong linkage between the KZI and energy inputs (T_{2m}) – as demonstrated in the main text – correlations between the KZI and streamflows (Figure 4E) strongly resemble those between energy inputs and streamflows (Supplementary Figure 1C). Specifically, glacial regime catchments show strong positive correlations whilst nival regime catchments show little relationship.

To be clear, this summary of hydrological regimes is not original (i.e. previously unpublished) research but a synopsis of a substantial body of existing work[9,10,11,12,15,16,30] (by the co-authors and their collaborators) for the convenience of readers of this publication.

Additional factors influencing glacial mass balance in the Karakoram and western HMA

Physiographic factors governing net glacial mass balance, beyond the climatological forcings driving glacial meltwater generation, are highly complex. In particular, two recent studies[7,8] have utilised multiple sources of remote sensing imagery to generate "snapshot" digital elevation models (DEMs) of Karakoram glacier surfaces for two or three points over the past several decades. Both studies found that key glaciers in the Karakoram were in a state of near equilibrium, i.e. showing weak/statistically insignificant positive or negative mass-balance changes, and, more specifically, substantial sub-regional heterogeneity[38,39]. Substantial technical resources were required to generate and assess even the limited (two or three time-step) surface elevation sequences, thus underlining the challenges in conducting comprehensive glacial mass-balance studies over an area as vast and varied as the Karakoram. Given the inherent challenges, an exhaustive exploration of Karakoram glacial mass-balance, and related climate forcings, is beyond the scope of this work.

A key factor which distinguishes Karakoram glaciers from those in other sub-regions of HMA is extensive debris cover, often with thickness greater than 1m on lower elevation tongues, and over substantial fractions of the total glaciated area[2,38,39]. In general, supraglacial debris reduces ablation (meltwater generation) by insulating the underlying ice from energy input, but when debris cover is very thin (~<3cm) ablation can actually be enhanced[38] possibly due to greater net shortwave absorption resulting from the lower albedo associated with thin debris cover, causing more efficient transmission of energy through the thin overlying layer. Untangling the complex factors dominating glacial mass balance, particularly when attempting to use glacial terminus position as proxy of mass change, is even more challenging when these factors interact. For example, debris cover can itself be driven by topographic factors, e.g. glacial slope both in accumulation zones and at glacier termini[39]. In particular, glacier topographic factors will strongly determine the amount of avalanche-driven mass transfer from accumulation to ablation zones[1]. In the Karakoram, separating climatic from physiographic factors is further complicated by the frequency of surge-type glaciers whose rates (and episodes) of advance may or may not be driven by climatological factors[2,40].

Separately, while the impact of thermal forcings – driven by atmospheric circulation conditions quantified by the KZI – on glacial ablation (meltwater generation) are clearly demonstrated in the present work (see Figure 4E,F and Supplementary Figure 1C) their impact on net glacial mass-balance cannot be established from the data available to the authors at this time. For example, Supplementary Figure 1C,E appears to suggest that melt season-concurrent (summer/JJA) energy and mass input climate forcings may well be (partially) coupled with warm and dry (wet and cold) conditions likely

to occur simultaneously during anticyclonic (cyclonic) episodes. In this context, upward (downward) movement of the freezing isotherm could yield greater liquid (solid) precipitation in ablation zones. In the cyclonic case (negative KZI), cold-wet conditions could both suppress ablation (meltwater generation) and increase accumulation at higher elevations, but at present we lack data to verify the latter (accumulation) component. For the time being we are limited to assessing the impacts of climate forcings on meltwater generation (Figure 4E,F and Supplementary Figure 1C,E).

Above all, observations of glacial thickness changes would be needed[2,40] – either from in-situ measurements or remote sensing –to rigorously establish the causality of factors suspected of driving net glacial mass-balance in HMA, including the thermal forcing driven by the KZI.

Exploration of broader geographic patterns in U (zonal wind) and T_{2m} anomalies by KZI phase

We now use ERA-interim reanalysis to explore relationships between the KZI and T_{2m}. Supplementary Figure 2 shows that in winter, the influence of the westerly jet extends throughout Eurasia for both strongly positive (>75th percentile) and strongly negative (<25th percentile) KZI, and resultant T_{2m} anomalies are spatially homogeneous, extending from the eastern Sahara to the China Sea. The sign of T_{2m} anomalies over South Asia is the same as that of zonal wind (U) in the northern KZI area. This indicates warm (cool) conditions during northward (southward) jet shifts. In contrast, in summer the northern branch of 200-hPa zonal wind speed anomalies is homogeneous only to the west of Mongolia, as its influence is disrupted by monsoonal development. T_{2m} anomalies mirror this pattern: Karakoram and western-HMA anomalies have the same sign as the KZI, but T_{2m} anomalies over the Indo-Gangetic plains and eastern-HMA show the opposite sign, i.e. the anomalous northward summer jet shift is concurrent with anomalously warm Karakoram and cool Ganges basin conditions. The highest positive and lowest negative KZI cases for both winter and summer show the same pattern (Supplementary Figure 3).

Data from global meteorological reanalyses

We use data from five reanalyses covering a range of time-periods: ERA-40[41] (September 1957 to August 2002), ERA-Interim[42] (January 1979 to near present), JRA-55[43] (September 1957 to near present), NASA MERRA[44] (January 1979 to near present), and NCEP CFSR[45] (January 1979 to December 2009). Only full years of reanalysis data from each ensemble member were included. We did not consider data after December 2010 as this was the end of the local Karakoram observational record available to the study. Thus, the "common record period" (of "full years") for the reanalysis ensemble and observations was from January 1979 to December 2001. In developing this study we drew on both reanalysis estimates of circulation variables (200-hPa Uwind, 500-hPa Uwind, etc.) and of near surface air temperature (T_{2m}).

To derive the zonal wind (U) climatologies of the northern (Unorth) and southern (Usouth) component areas of the KZS, spatial mean values for each time-step from each reanalysis were calculated by a weighted averaging of all grid cells overlying the individual target domain (defined by area boundaries, Figure 1A, main text). Where edges were overlain by partial grid cells, weighting was performed by calculating the fraction of each reanalysis grid cell overlying the target domain.

This process was repeated to derive the reanalysis estimates of T_{2m} for the Karakoram as a whole. Following the extraction of absolute value estimates for T_{2m}, we have chosen to work with near surface air temperature estimates solely in "anomaly space" (standardisation by subtraction of period mean then division by period standard deviation). The aim of this was to remove as much as possible the potential "entrainment" of bias from such effects such as the inclusion by ERA-Interim of a 10m thick ice layer in grid cells with >50% glaciation[46]. We deal with temperature estimates from

reanalyses as either point extractions from within individual grid cells or as fixed spatial aggregates. In both cases extracted values are directly standardised (subtraction of period mean, division by standard deviation). They are thus considered purely in terms of their temporal patterns of variability relative to their own statistical distributions rather than in terms of physical values relatable to fixed thresholds (e.g. freezing) or difference-driven processes (e.g. sensible heat flux). Spatial aggregation was performed, using the NW UIB boundary shown in Figure 1A, in order to test the ability of each reanalysis to replicate T_{2m} response to large-scale circulation forcing.

Local T_{2m} observation stations

Temperature data were obtained from the Pakistan Meteorological Department (PMD) via the Global Climate Impact Studies Centre (GCISC) and from the Global Historical Climate Network (GHCN) database version 3.2[47]. Data obtained from PMD/GCISC was at a daily time-step and aggregated by the authors to monthly means. GHCN data was obtained as monthly means. Supplementary Table 1 provides the location, surface elevation and data provenance for the local observational stations used in this study.

Observations of Upper Indus tributary catchments' river discharge

Observations of discharge (streamflow) from Upper Indus basin tributary catchments are carried out by the Pakistan Water and Power Development Authority (WAPDA) through a network of gauging stations. The authors gained access to this data both directly from WAPDA staff (past and present) and through partner researchers including the Global Climate Impact Studies Centre (GCISC). Delineation of Indus tributary catchments is based on the work of Khan et al[48] who kindly provided the GIS (vector/shape) files used in Supplementary Figure 1A. Locations for WAPDA gauging sites, also shown in Supplementary Figure 1A, were digitised based on Archer[10]. Estimated spatial distribution of glaciated area is based on the Randolph Glacier Inventory (version 5.0)[49,50].

Delineation of KZS influence zones and derivation of KZS climatology

Drawing on an approach used to assess atmospheric circulation influences on Himalayan winter precipitation[20,21], we produced a semi-global exploration of correlations between key circulation variables and Karakoram T_{2m} observations at three multi-decadal record stations previously used to identify anomalous summer cooling[9]: Astore, Gilgit and Skardu (see Supplementary Table 1). We computed grid-cell wise correlations of T_{2m} observations from these 3 stations with 200-, 500- and 700-hPa geopotential heights and zonal and meridional wind speeds, mean sea level pressure and net longwave (thermal) radiation at the surface as quantified in ECMWF reanalyses, ERA-40[41] and ERA-Interim[42]. We identified two areas of zonal (westerly) circulation with strong influence over Karakoram T_{2m} variability (see Supplementary Figure 5) based on a correlation threshold of 0.30 at both 200- and 500-hPa. These atmospheric layers provide a core delimitation of the atmospheric jet streams in proximity to HMA[51]. We simplified the irregular areas shown in Supplementary Figure 5 to rectangular shapes as shown in Figure 1A (inset). The respective bounds of the northern and southern areas are: a) 40N to 50N, 52.5E to 86.25E; and b) 20N to 32.5N, 52.5E to 93.75E. Thus:

$$\mathrm{KZS} = \overline{\mathrm{U}}_{(40^\circ\ \mathrm{N\ to\ 50^\circ\ N,\ \ 52.5^\circ\ E\ to\ 86.25^\circ\ E})} - \overline{\mathrm{U}}_{(20^\circ\ \mathrm{N\ to\ 32^\circ\ N,\ \ 52.5^\circ\ E\ to\ 93.75^\circ\ E})}.$$

The derived KZS climatologies shown in Figure 1B are based on sampling of the spatial means calculated from individual reanalysis ensemble members.

We find general agreement between the component influence areas delineated with 200- and 500-hPa level wind speeds respectively from ERA-40 (Supplementary Figure 5A) and ERA-Interim (Supplementary Figure 5B). Visually, the difference in spatial resolution, i.e. 2.5 decimal degrees in

ERA-40 and 0.75 decimal degrees in ERA-Interim, of the two reanalyses appears to play a substantial role in the subtly different shapes of delineated zones. We did not perform a sensitivity analysis to assess the influence of varying the correlation strength threshold (0.30). However, very limited spread among the KZS climatologies within the reanalysis ensemble (main text Figure 1A, 1B) led us to conclude that minor variations in the geographic definition of the areas of influence would have minimal influence on the physical interpretation of the findings of this study.

Reanalysis-ensemble T_{2m} proxy data validation

To provide a reanalysis-ensemble proxy value for an observed station location (point), the grid cell overlying the station from each individual reanalysis was extracted and standardised by subtracting period monthly mean, and dividing by period monthly standard deviation to calculate standardised monthly anomaly time-series. The ensemble mean of these anomalies then provided the reanalysis-ensemble value. For time-periods outside the common record, the mean standardised value was calculated using the available ensemble members.

To validate the use of reanalysis ensemble proxies for missing data values in T_{2m} observations and unavailable station datasets, we evaluated the relationships between available T_{2m} observations and individual reanalyses detailed above. Correlations were measured using the Pearson moment coefficient 'r'. Supplementary Table 2 shows the Pearson correlations between individual reanalyses and T_{2m} observations. For stations with both national agency and GHCN provenance, with the exception of a single station record – for Quetta from GHCN – all correlations between individual stations and individual reanalyses are greater than 0.50. Pearson correlations greater than 0.90 are found for some dual provenance stations and JRA-55. Differences in correlation strength with individual reanalyses between GHCN-derived and national institution data sources for the same stations were in all cases less than 0.10. Pearson correlation statistics between single-source station data and reanalyses generally show the same patterns – i.e. strongest correlations to ERA-Interim and JRA-55, weakest to NCEP CFSR – as do those with dual (both GHCN and national institution) sources. While the overall pool of stations show slight variability in correlation strengths, Pearson correlations greater than 0.70 are frequent. In general, the reanalysis ensemble members that provided the best correlations to local observations were JRA-55 and ERA-Interim.

Numerical methods for time-series and gridded data analyses

In conducting the work presented here we drew upon a wide range of software packages for calculation of relevant statistics. Linear regressions and Kendall Tau correlations were performed using Numerical Python[52] (NumPy) respectively through the "ols" and "scipy.stats" modules. Compositing and Pearson correlations on variables from the (gridded) ERA-Interim reanalysis were performed with a mixture of NCAR command language[53] (NCL) and NumPy scripting procedures. NumPy gridded data processing specifically utilised the "Scientific.IO"[54] and "rasterIO"[55] modules.

Data availability

The data used – analysed and generated – in this study fall into three categories of availability. Global, publicly available datasets were obtained from web-based platforms maintained by their producers. These include global meteorological reanalyses – ERA-40[41], ERA-Interim[42], JRA-55[43,56], NASA MERRA[44] and NCEP CFSR[45,57] – and the GHCNv3.2 monthly air temperature dataset[47]. The datasets of local observations (air temperature, streamflow) are available from PMD and WAPDA but restrictions apply to the availability of these data, which were used under license for the current study, and so are not publicly available. Data are however available from the authors upon reasonable

request and with permission of PMD and/or WAPDA. Data, specifically time-series of KZS and KZI and reanalysis proxies of station and spatial aggregate T_{2m}, derived from the analysis of global datasets are available from the corresponding author on request.

REFERENCES (METHODS)

[38] Mihalcea, C., Mayer, C., G. Diolaiuti, D'Agata, C., Smiraglia, C., Lambrecht, A., Vuillermoz, E., and Tartari, G., 2008. Spatial distribution of debris thickness and melting from remote-sensing and meteorological data, at debris-covered Baltoro Glacier, Karakoram, Pakistan, *Ann. Glaciol*., **48** (1), 49–57. http://dx.doi.org/10.3189/172756408784700680

[39] Scherler, D., Bookhagen, B. and Strecker, M.R., 2011. Spatially variable response of Himalayan glaciers to climate change affected by debris cover. *Nature Geoscience*, **4** (3), 156-159. http://dx.doi.org/10.1038/NGEO1068

[40] Heid, T. and Kääb, A., 2012. Repeat optical satellite images reveal widespread and long term decrease in land-terminating glacier speeds. *The Cryosphere*, **6**, 467-478, http://dx.doi.org/10.5194/tc-6-467-2012

[41] Uppala, S.M. et al, 2005. The ERA-40 re-analysis. *Quarterly Journal of the Royal Meteorological Society* **131** (612) 2961-3012. http://dx.doi.org/10.1256/qj.04.176

[42] Dee, D.P., Uppala et al, 2011. The ERA-Interim reanalysis: configuration and performance of the data assimilation system. *Q. J. R. Meteorol. Soc*. **137** (656), 553–597. http://dx.doi.org/10.1002/qj.828

[43] Ebita, A. et al, 2011. The Japanese 55-year Reanalysis "JRA-55": An Interim Report. *Scientific Online Letters on the Atmosphere*, **7**, 149-152. http://dx.doi.org/10.2151/sola.2011-038

[44] Rienecker, M.M. et al, 2011. MERRA: NASA's modern-era retrospective analysis for research and applications. *Journal of Climate*, **24** (14), 3624-3648. http://dx.doi.org/10.1175/JCLI-D-11-00015.1

[45] Saha, S. et al, 2011. The NCEP climate forecast system reanalysis. *Bulletin of the American Meteorological Society*, **91** (8), pp. 1015-1057. http://dx.doi.org/10.1175/2010BAMS3001.1

[46] Collier, E., Mölg, T., Maussion, F., Scherer, D., Mayer, C., Bush, A.B.G. and Immerzeel, W.W., 2013. High-resolution interactive modelling of the mountain glacier–atmosphere interface: an application over the Karakoram. *The Cryosphere.*, **7** (3), 779–795, http://dx.doi.org/10.5194/tc-7-779-2013

[47] Lawrimore, J.H. et al, 2011. An overview of the Global Historical Climatology Network monthly mean temperature data set, version 3. *Journal of Geophysical Research: Atmospheres*, **116** (19), D19121. http://dx.doi.org/10.1029/2011JD016187

[48] Khan, A., Richards, K.S., Parker, G.T., McRobie, A. and Mukhopadhyay, B., 2013. How large is the Upper Indus Basin? The pitfalls of auto-delineation using DEMs. *Journal of Hydrology*, **509**, 442-453, http://dx.doi.org/10.1016/j.jhydrol.2013.11.028.

[49] Arendt, A. et al., 2015, Randolph Glacier Inventory – A Dataset of Global Glacier Outlines: Version 5.0. Global Land Ice Measurements from Space, Boulder Colorado, USA. Digital Media. http://www.glims.org/RGI/00_rgi50_TechnicalNote.pdf

[50] Pfeffer, W.T. et al., 2014. The randolph glacier inventory: A globally complete inventory of glaciers. *Journal of Glaciology*, **60** (221), 537-552. http://dx.doi.org/10.3189/2014JoG13J176

[51] Maussion, F., Scherer, D., Mölg, T., Collier, E., Curio, J. and Finkelnburg, R., 2014. Precipitation seasonality and variability over the Tibetan Plateau as resolved by the high Asia reanalysis. *Journal of Climate*, **27** (5), pp. 1910-1927. http://dx.doi.org/10.1175/JCLI-D-13-00282.1

[52] Oliphant, T.E., 2007. Python for scientific computing. Computing in Science and Engineering, 9 (3), art. no. 4160250, 10-20. http://dx.doi.org/10.1109/MCSE.2007.58

[53] The NCAR Command Language (Version 6.4.0) [Software]. (2017). Boulder, Colorado: UCAR/NCAR/CISL/TDD. http://dx.doi.org/10.5065/D6WD3XH5

[54] Hinsen K. (2002) High-Level Scientific Programming with Python. In: Sloot P.M.A., Hoekstra A.G., Tan C.J.K., Dongarra J.J. (eds) Computational Science — ICCS 2002. ICCS 2002. Lecture Notes in Computer Science, vol 2331. Springer, Berlin, Heidelberg http://dx.doi.org/10.1007/3-540-47789-6_72

[55] Holderness, T. 2011. Python Spatial Image Processing (PyRaster). https://github.com/talltom/PyRaster

[56] JRA-55: Japanese 55-year Reanalysis, Daily 3-Hourly and 6-Hourly Data. Accessed via the Research Data Archive (RDA), managed by the Data Support Section (DSS) of the Computational and Information Systems Laboratory (CISL) at NCAR (ds628.0). DOI: 10.5065/D6HH6H41

[57] NCEP Climate Forecast System Reanalysis (CFSR) 6-hourly Products, January 1979 to December 2010. Accessed via the Research Data Archive (RDA), managed by the Data Support Section (DSS) of the Computational and Information Systems Laboratory (CISL) at NCAR (ds093.0). DOI: 10.5065/D69K487J

SUPPLEMENTARY INFORMATION for **Karakoram temperature and glacial melt driven by regional atmospheric circulation variability**

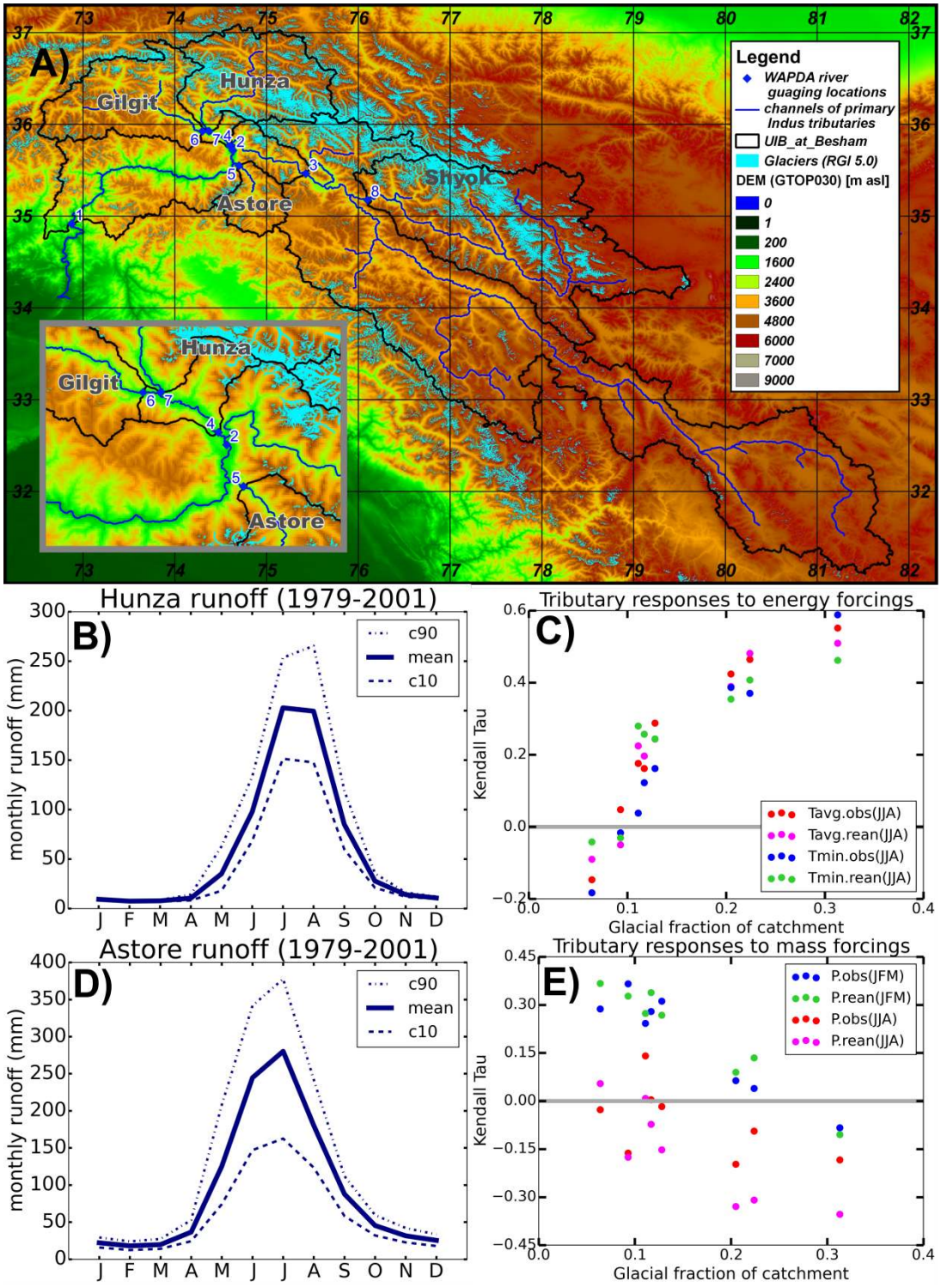

[Supplementary Figure 1] Illustrations of the hydro-climatology of Upper Indus tributaries. A) Boundaries and gauging locations of Upper Indus tributary catchments: 1) Indus to Besham, 2) Indus to Partab bridge, 3) Indus to Kachura, 4) Gilgit/Ghizer to Alam Bridge, 5) Astore to Doyian, 6) Gilgit/Ghizer to Gilgit town, 7) Hunza to Dainyor Bridge, 8) Shyok to Yogo. Annual cycles of streamflow (as runoff) from Indus tributaries representative of key hydrological regimes: "glacial" regime at Hunza (B) and "nival" regime at Astore (D). Climatological controls (as Mann-Kendall tau correlations) on streamflow from Indus tributaries with respect to glaciated fraction of catchment area: C) energy forcings, i.e. T_{2m}; E) mass forcings, i.e. precipitation. In panels C and E climate forcings are quantified both using local observations {suffix ".obs"} (in the same manner as in Figure 4) and reanalysis ensemble standardised estimates {suffix ".rean"} of a spatial mean over the northwest Upper Indus basin (shown in red in Figure 1A).

[Supplementary Table 1] Local observation station coordinates, surface elevation and data provenance. Automatic weather stations (AWS) are operated by the Pakistan Water and Power Development Authority (WAPDA). Data for stations operated by the Pakistan Meteorological Department (PMD) was acquired via the Global Change Impact Studies Centre (GCISC). Some data was available in parallel through the Global Historical Climate Network (GHCN). "Reanalysis ensemble proxy" data was calculated from an ensemble of global meteorological reanalyses

Station	**Latitude**	**Longitude**	**Elevation**	**Data provenance**
Khunjerab	36.85	75.40	4733	AWS (WAPDA)
Ziarat	36.47	75.15	3688	AWS (WAPDA)
Naltar	36.13	74.18	2810	AWS (WAPDA)
Gilgit	35.92	74.33	1460	PMD (GCISC)
Chitral	35.85	71.83	1499	PMD (GCISC)
Drosh	35.57	71.78	1465	PMD (GCISC)
Astore	35.36	74.90	2394	PMD (GCISC)
Skardu	35.30	75.68	2210	PMD (GCISC)
Saidu Sharif	34.75	72.35	961	PMD (GCISC)
Muzzaferabad	34.35	73.46	686	PMD (GCISC)
Islamabad	33.71	73.06	519	PMD (GCISC)
Kohat	33.58	71.43	501	PMD (GCISC)
Sialkot	32.49	74.53	256	PMD (GCISC)
Faisalabad	31.41	73.07	186	PMD (GCISC)
Zhob	31.35	69.45	1405	PMD (GCISC)
Jhelum	32.92	73.73	234	dual (PMD & GHCN)
Lahore	31.54	74.34	215	dual (PMD & GHCN)
Quetta	30.21	67.01	1673	dual (PMD & GHCN)
Multan	30.19	71.46	163	dual (PMD & GHCN)
Dalbandin	28.88	64.41	850	dual (PMD & GHCN)
Jacobabad	28.27	68.45	56	dual (PMD & GHCN)
Hyderabad	25.37	68.36	41	dual (PMD & GHCN)
Karachi	24.86	67.01	22	dual (PMD & GHCN)
Srinagar	34.00	74.76	1587	GHCN
Shimla	31.10	77.15	2202	GHCN
New Delhi	28.58	77.20	216	GHCN
Kathmandu	27.70	85.37	1337	GHCN
Leh	34.14	77.56	3506	reanalysis ensemble proxy
Mustang	29.18	83.97	3705	reanalysis ensemble proxy
Dhangadi	28.68	80.60	1360	reanalysis ensemble proxy
Chisapani	28.65	81.27	225	reanalysis ensemble proxy
Gorkha	28.00	84.62	1097	reanalysis ensemble proxy
Rampur	27.62	84.42	256	reanalysis ensemble proxy
Chialsa	27.52	86.62	2770	reanalysis ensemble proxy
Taplejung	27.35	87.67	1732	reanalysis ensemble proxy

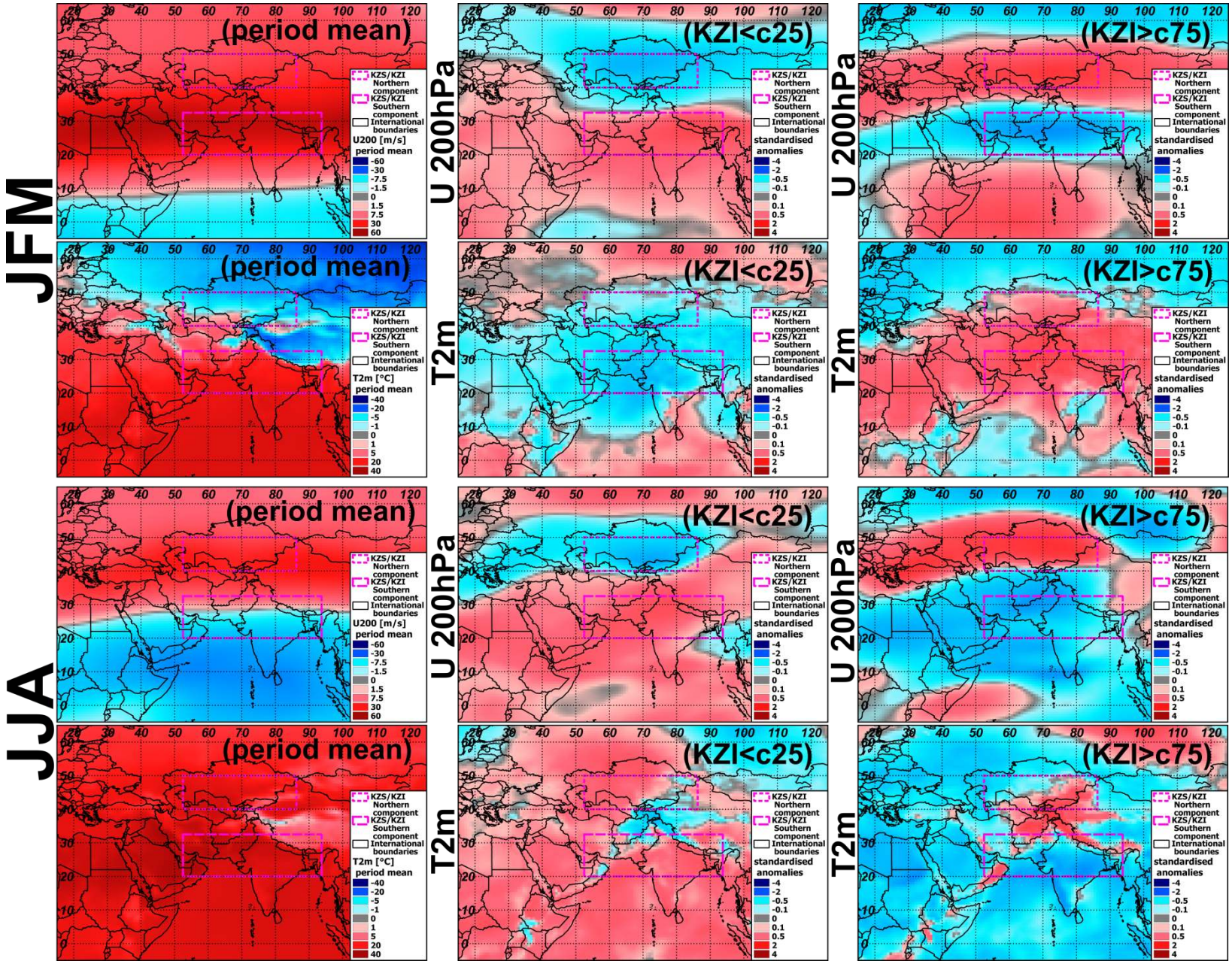

[Supplementary Figure 2] Composite (gridded cell-wise) standardised anomalies of 200-hPa zonal wind speeds (Uwind) and near surface air temperature (T_{2m}) for winter (JFM) and summer (JJA) seasons for 1979-2012, as estimated by ERA-Interim. Anomalies are composited by rank of the individual season within the KZI observational distribution. Seasons ranked in the upper quartile (KZI>c75) of the KZI record for a given season (JFM or JJA) are averaged as are values for the lower quartile years (KZI<c25).

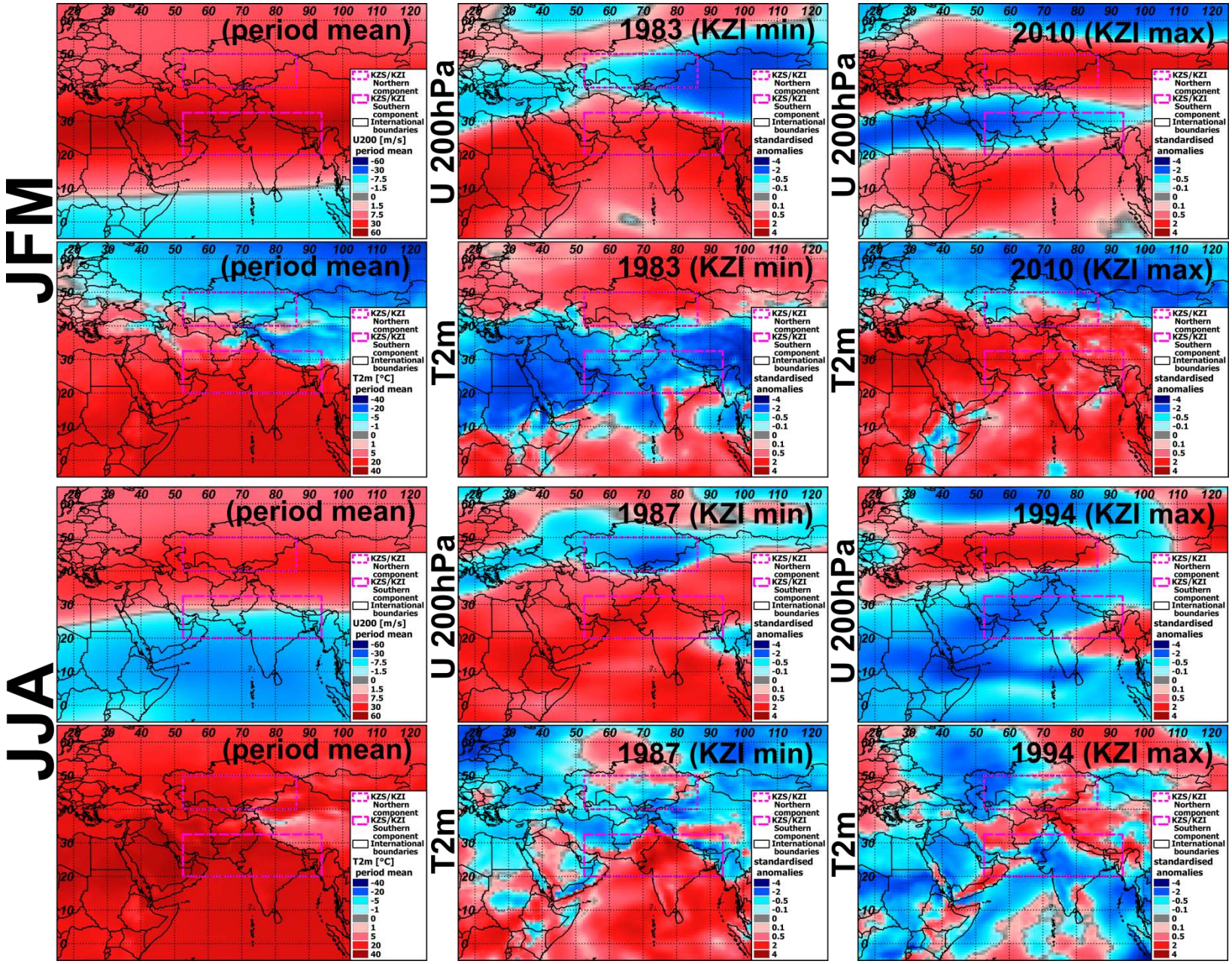

[Supplementary Figure 3] Standardised anomalies of 200-hPa zonal wind speeds (Uwind) and near surface air temperature (T_{2m}) for winter (JFM) and summer (JJA) seasons, as estimated by ERA-Interim. Results shown for highest positive (max) and lowest negative (min) KZI cases for both winter and summer from the period 1979-2012.

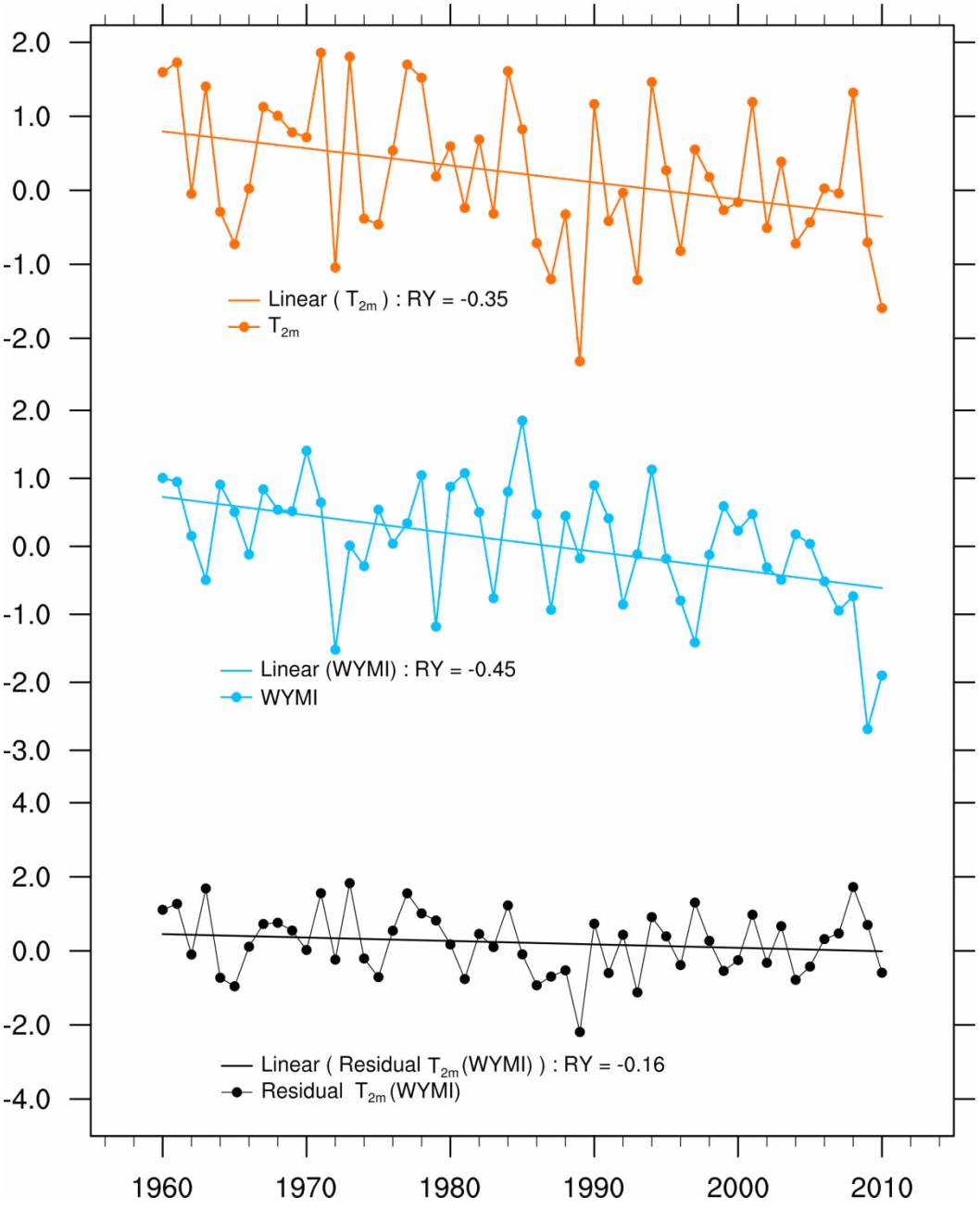

[Supplementary Figure 4] |Contributions of the Indian Summer Monsoon (ISM) atmospheric circulation to the cooling of 2m surface air temperature (T_{2m}) over the Karakoram: (top) Karakoram summer (JJA) T_{2m}; (middle) the WYMI, used as a metric for ISM circulation strength; (bottom) time series of residual T_{2m} from the value predicted with linear regression using time series of WYMI. Linear trends are shown for all variables as straight real line. "RY" is the trend correlation coefficient.

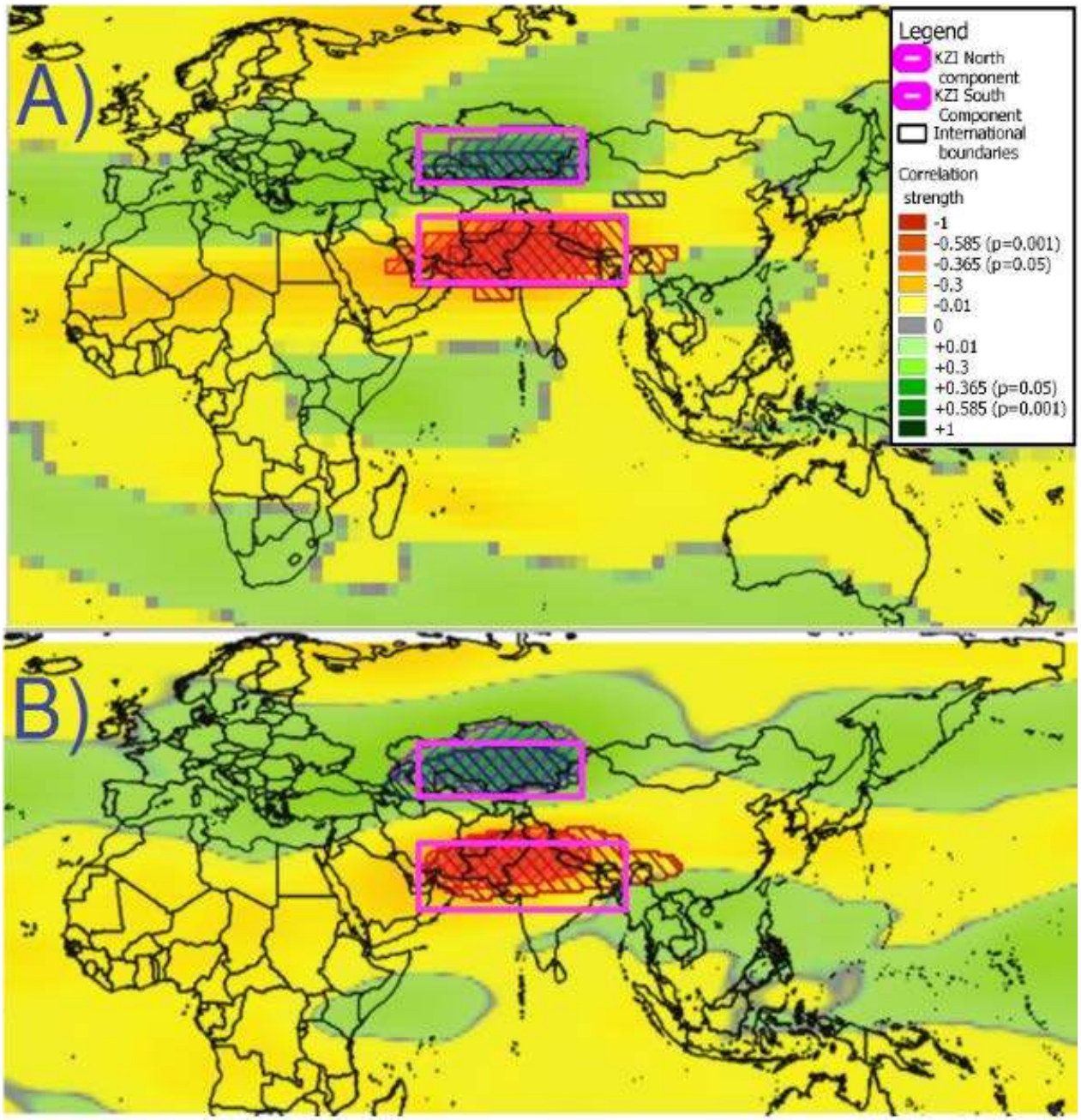

[Supplementary Figure 5] Composite of "Grid cell-to-point" correlations of U (i.e. zonal wind) with T_{2m} from 3 long record Karakoram meteorological stations – Gilgit, Skardu and Astore – which provided the basis for definition of KZI areas of influence: A) ERA-40; B) ERA-Interim. The colour scale indicates the correlation strength between 200-hPa zonal wind and Karakoram T_{2m}. Purple and brown boundaries delineate the northern and southern influence areas respectively for 200-hPa zonal wind while blue and red boundaries delineate the northern and southern influence areas for 500-hPa zonal wind.

[Supplementary Table 2] Pearson correlations between local T_{2m} observations and reanalysis T_{2m} estimates for stations. Data for the first eight stations were available from both GHCN and national institution (PMD) data provenance. Remaining stations were available from a single source.

Station	Inter-source correlation	Source type	Individual reanalyses				
			ERA-40	JRA-55	ERA-Interim	NCEP CFSR	NASA MERRA
Jhelum	0.993	GHCN	0.614	**0.909**	0.881	0.774	0.707
		GCISC	0.619	***0.910***	0.884	0.772	0.706
Lahore	0.967	GHCN	0.678	**0.883**	0.863	0.719	0.705
		GCISC	0.649	***0.896***	0.875	0.723	0.696
Multan	0.937	GHCN	0.722	0.768	**0.801**	0.737	0.724
		GCISC	0.790	0.831	***0.855***	0.804	0.788
Jacobabad	0.889	GHCN	0.651	0.744	0.725	***0.778***	0.688
		GCISC	0.607	0.697	0.651	**0.727**	0.654
Dalbandin	0.972	GHCN	0.717	0.731	***0.833***	0.795	0.673
		GCISC	0.710	0.711	**0.819**	0.799	0.698
Hyderabad	0.834	GHCN	0.599	**0.839**	0.760	0.754	0.687
		GCISC	0.531	***0.842***	0.784	0.746	0.702
Quetta**	0.189**	GHCN**	0.124	**0.161**	0.125	0.027	0.086
		GCISC	***0.779***	0.717	0.698	0.648	0.540
Karachi	0.968	GHCN	0.661	**0.770**	0.660	0.766	0.716
		GCISC	0.658	0.756	0.674	***0.803***	0.725
Srinagar		GHCN	0.727	**0.770**	0.570	0.516	0.481
Shimla		GHCN	0.651	0.627	0.676	0.681	**0.726**
New Delhi		GHCN	0.857	**0.933**	0.891	0.879	0.652
Kathmandu		GHCN	0.529	**0.622**	0.571	0.544	0.527
Khunjerab		WAPDA	**0.667**	0.573	0.575	0.624	0.652
Ziarat		WAPDA	0.570	0.505	**0.608**	0.466	0.577
Naltar		WAPDA	0.640	0.619	**0.739**	0.571	0.732
Gilgit		PMD/GCISC	0.701	0.650	**0.707**	0.456	0.684
Skardu		PMD/GCISC	0.616	0.593	**0.675**	0.443	0.673
Astore		PMD/GCISC	0.720	0.672	**0.763**	0.464	0.738
Chitral		PMD/GCISC	**0.702**	0.487	0.538	0.399	0.662
Drosh		PMD/GCISC	0.580	0.515	0.538	0.392	**0.598**
Saidu Sharif		PMD/GCISC	0.545	**0.674**	0.658	0.460	0.635
Muzzafferabad		PMD/GCISC	0.456	**0.806**	0.715	0.621	0.635
Islamabad		PMD/GCISC	0.680	**0.851**	0.786	0.773	0.726
Kohat		PMD/GCISC	0.662	**0.691**	0.597	0.600	0.644
Sialkot		PMD/GCISC	0.534	0.434	**0.863**	0.685	0.690
Faisalabad		PMD/GCISC	0.668	**0.849**	0.841	0.801	0.714
Zhob		PMD/GCISC	0.685	0.772	**0.794**	0.580	0.688

Formatting notes for **[Supplementary Table 2]**: **bold** indicates best correlation within a row (data source versus reanalysis); ***bold italic*** indicates best overall correlation for a station between its T_{2m} observational record and the overlying T_{2m} estimates from an individual reanalysis.

** These low correlations may be an issue of GHCN versus GCISC station identification "Quetta / Samungli" versus "Quetta Cantonment", stations are at approximately same elevation and separated by 15km.

Correlations of large-scale atmospheric modes and Karakoram T_{2m}

To illustrate the relative value of the Karakoram Zonal Index (KZI) in characterising Karakoram near surface air temperature (T_{2m}) for the period 1979-2001, we correlated the KZI and T_{2m} for winter and summer respectively using Kendall's tau (τ). The results for winter and summer, respectively, are $\tau = 0.423$ ($p=0.005$) and $\tau = 0.450$ ($p=0.003$). These correlations to Karakoram T_{2m} are substantially stronger than those for other large-scale atmospheric circulation modes. The winter and summer correlations between the North Atlantic Oscillation (NAO)[1,2] and Karakoram T_{2m} are respectively $\tau = -0.275$ ($p=0.066$) and $\tau = 0.060$ ($p>0.5$). For the El Niño Southern Oscillation (ENSO)[3], represented by the Multivariate ENSO Index (MEI)[4] for winter and summer respectively, correlations are $\tau = -0.310$ ($p=0.038$) and $\tau = 0.036$ ($p>0.5$). For summer season correlations, the skill of the KZI is also greater than that of the Webster and Yang Monsoon Index (WYMI)[5] of South Asian summer monsoonal circulation: $\tau = 0.301$ ($p=0.044$) for 1979-2001 and $\tau = 0.304$ ($p=0.0016$) for 1960-2010 – despite it spanning a similar longitudinal range with its influence area and it being adjacent to the KZI southern component zone over peninsular India. For context, the correlations between the summer (JJA) KZI and the WYMI are $\tau = 0.380$ ($p=0.0111$) for 1979-2001 and $\tau = 0.411$ ($p<0.0001$) for 1960-2010. We interpret these results as showing that, while westerly jet influence on summer temperatures over the Karakoram and the South Asian monsoonal circulation are certainly linked, the KZI provides substantially greater information content than a purely monsoonal circulation metric. This is both by utilising zonal winds from higher pressure levels (200- or 500-hPa) and by incorporating the northern influence area (over Central Asia, east of the Caspian Sea) rather than over the Indian Ocean – relevant to characterising large-scale circulation effects on HMA near-surface conditions.

Karakoram summer (JJA) T_{2m} has experienced statistically significant cooling since the 1960s (Supplementary Figure 4). The Pearson correlation with time (years) is -0.35 ($p<0.05$). We now consider the extent to which this could be attributed to the weakening of the South Asian summer monsoonal circulation which we are quantifying using the Webster and Yang Monsoon Index (WYMI)[5]. The weakening of the South Asian summer monsoon in recent decades has been widely reported[6,7,8]. This is numerically demonstrated by the Pearson correlation of WYMI with time (years) of -0.45 (Supplementary Figure 4). The Pearson correlation between Karakoram summer (JJA) T_{2m} and the WYMI – after the removal of linear (temporal) trends – is 0.37 ($p<0.05$). This substantiates an intrinsic connection with T_{2m}. As the South Asian summer monsoonal circulation is coupled with the south branch of the Karakoram Vortex (KV), the weakening of the monsoon is also quantified by progressively rarer negative anomalies in the KZI southern component area (main text, Figure 4D). Thus the dynamic mechanism linking monsoonal weakening to Karakoram cooling is the shift of the KV toward cyclonic (negative KZI) conditions. This is illustrated in the bottom panel of Supplementary Figure 4: after removing the influence of the WYMI by subtracting T_{2m} predictands calculated by linear regression, the trend in the residual T_{2m} is reduced to near zero, i.e. the Pearson correlation with time index equals -0.16 (statistically insignificant). This indicates that there is no significant cooling trend after accounting for the synchronisation with the monsoonal circulation.

This strongly suggests that the cooling trend in Karakoram summer (JJA) T_{2m} linked to the KZI (main text Figure 4B) is attributable to the drivers also causing the recent weakening of the South Asian summer monsoonal circulation.

Along these lines, when we refer to Supplementary Figure 3 which shows the maximum and minimum case (years) of KZI for both winter (JFM) and summer (JJA), we see that:

- The maximum KZI winter case occurred in 2010. This was a moderate and declining El Niño event (Jan to May).
- The minimum KZI winter case occurred in 1983. This was a very strong El Niño event.
- The maximum KZI summer case occurred in 1994. This coincided with a weak (small positive MEI) El Niño event but a strong (1.13) WYMI value for monsoonal circulation.
- The minimum KZI summer case occurred in 1987. This coincided with a strong El Niño event and very weak (-0.93) WYMI value indicating a poorly developed monsoon.

The complexity of these relationships between KZI and ENSO and, in summer, WYMI indicate both challenges and priorities for future research to identify and characterise driving large-scale mechanisms of the KV and KZI variability. We have already established the strong WYMI-KZI linkage in summer, but attributing, via atmospheric processes, the "levers" by which other large-scale atmospheric modes – ENSO, NAO, Arctic Oscillation[9,10] (AO), etc – act upon the KV and KZI state will require substantial investigation, including detailed consideration of atmospheric dynamics.

Further discussion on causal mechanisms of KZI-T_{2m} response

In addition to the vertical motion (adiabatic cooling/warming) mechanism described in the main text, surface radiation balance effects are also associated with various KZI states. A positive KZI anomaly in summer indicates strong monsoonal development. In the south and east of the domain, this could be associated with reduced surface insolation, and hence diminished diurnal warming, due to extensive cloud cover. A negative summer KZI, in contrast, indicates weak monsoonal development which fails to push the westerly jet northward. The resulting relatively cloud-free (anticyclonic) conditions over eastern HMA and the Indo-Gangetic plains could yield increased insolation and enhanced diurnal warming. In contrast, in the Karakoram (northwest of study domain) more complex conditions may prevail. A positive summer KZI would indicate greater than normal encroachment or penetration of monsoonal circulation into the Karakoram. Given that this results in a warm temperature anomaly, it could be inferred that substantial warm air is advected into the area. In contrast, a negative KZI would imply that (absolute) summer circulation conditions (KZS) are closer to those in spring and autumn (see main text Figure 1B) when the Karakoram generally experiences greater cloud cover[11]. This suggests that a negative KZI may cause increased summer cloud cover and decreased insolation in the Karakoram, consistent with more frequent passage of extra-tropical westerly depressions which are normally pushed northward by the progression of monsoonal circulation. This is supported by previous findings[12] indicating that weakened South Asian monsoonal circulation (which we link to negative KZI anomalies) corresponds with anomalously cyclonic (logically cloudier) circulation patterns over western HMA. Zhao et al.[12] further identified substantial cold air advection into the sub-region under these conditions.

Decreased insolation would suppress diurnal warming and consequently cause reductions in glacial melt, particularly if coupled with cold air advection. Under this hypothesis, strong monsoonal development (positive summer KZI) would yield prevailing clear conditions in the Karakoram, due to northward displacement of the westerly jet, with resultant increased insolation and diurnal

warming. The tendency in recent years toward negative summer KZI states (main text Figure 4B) suggests that "low energy input" conditions have prevailed thus leading to reduced ablation and positive glacier mass balance, hence the "Karakoram Anomaly"[13]. Karakoram T_{2m} response to the KZI is of critical importance to glacier mass-balance in high elevation tributaries of the Indus. Previous studies[14,15,16] have established both the trend of summer Karakoram cooling in recent decades and its implications for decreased glacial meltwater contributions to Indus river flow.

KZI-T_{2m} relationships in reanalyses

Further evidence that reanalyses, in particular ERA-Interim[17], are able to reproduce KZI-T_{2m} relationships are shown in Supplementary Figures 6 and 7. The five derived Karakoram T_{2m} time-series from the individual reanalyses were tested for correlations against KZI as shown in Supplementary Figure 6A. Furthermore, since JRA-55[18] provides a long time record (1958 to near present), we split the JRA-55 record into two (slightly overlapping) 30-year time slices – 1958 to 1987, 1984 to 2013 – to test whether substantial differences are found based on the choice of (historical) time period. Supplementary Figure 6B shows that JRA-55 characterises KZI-T_{2m} relationships for the Karakoram as relatively stable during the historical period. While Supplementary Figure 7 was produced to validate the use of ensemble mean standardised T_{2m} estimates as proxies for filling occasional gaps from missing T_{2m} observational data, the figure also clearly shows that the ensemble of reanalyses accurately reproduces the (sub-)regional spatial patterns of KZI-T_{2m} relationships found using local observations.

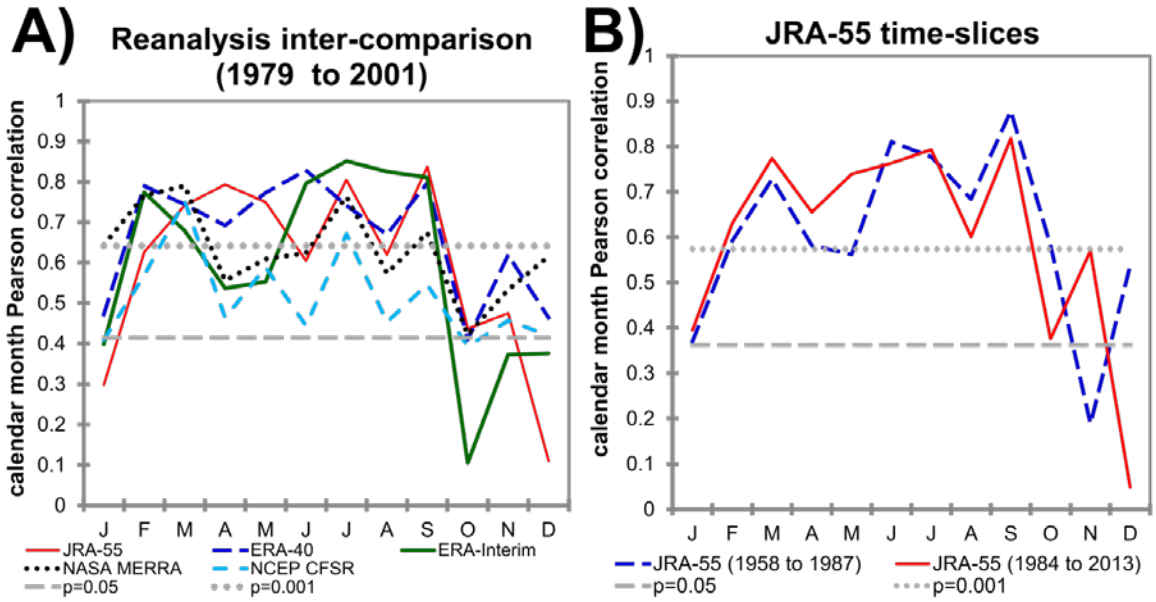

[Supplementary Figure 6] KZI influence on Karakoram surface air temperature (T_{2m}). The 'internal coherence' of reanalysis representations of the KZI- T_{2m} are explored through A) inter-comparison of ensemble member correlations for a common period, 1979-2001, and B) 'time-slice' comparison of correlations within the JRA-55 reanalysis.

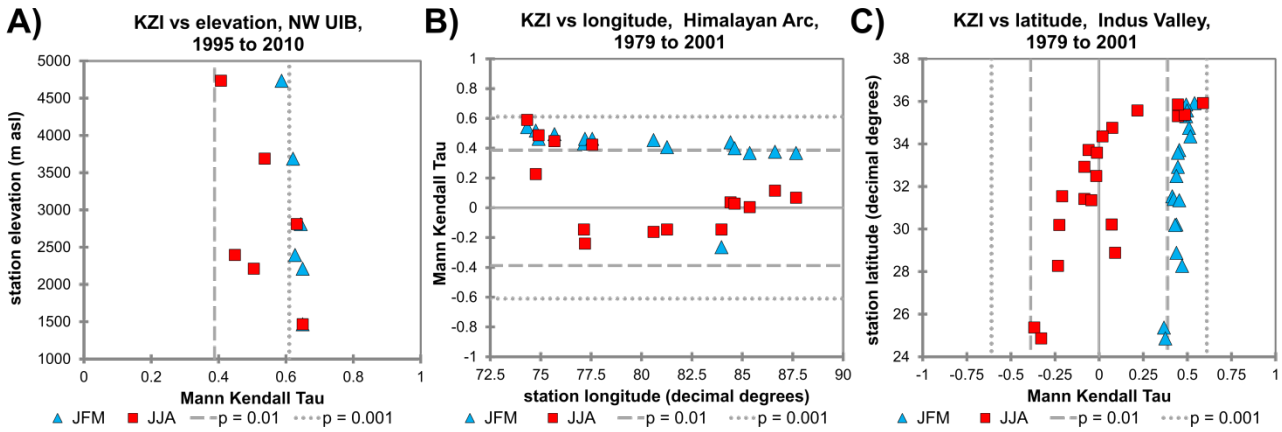

[Supplementary Figure 7] Seasonal correlations between the KZI and reanalysis ensemble estimates of T_{2m} along transects: A) vertical, 1500m to 4500m a.s.l., 1995-2010, B) longitudinal, ~74°E to 87.5°E, 1979-2001, and C) latitudinal, ~25°N to 36°N,1979-2001. Stations are shown in Figure 1A: A) vertical transect stations within the NW UIB (red boundaries); time-period differs as AWS records are only available from 1995; B) Himalayan arc transect stations along the blue dashed line (H.A.); C) Indus Valley transect stations along the magenta dashed line (I.V.).

REFERENCES (SUPPLEMENTARY INFORMATION)

[1] van den Dool, H.M., Saha, S. and Johansson, A., 2000. Empirical Orthogonal Teleconnections. *J. Climate*, **13**, 1421-1435. http://dx.doi.org/10.1175/1520-0442(2000)013<1421:EOT>2.0.CO;2

[2] Barnston, A. G., and R. E. Livezey, 1987: Classification, seasonality and persistence of low-frequency atmospheric circulation patterns. *Mon. Wea. Rev.*, **115**, 1083-1126. http://dx.doi.org/10.1175/1520-0493(1987)115<1083:CSAPOL>2.0.CO;2

[3] Trenberth, K.E., 1997. The Definition of El Niño. *Bulletin of the American Meteorological Society*, **78**, 2771-2777. http://dx.doi.org/10.1175/1520-0477(1997)078<2771:TDOENO>2.0.CO;2

[4] Wolter, K. and Timlin, M.S., 2011. El Niño/Southern Oscillation behaviour since 1871 as diagnosed in an extended multivariate ENSO index (MEI.ext). *Intl. J. Climatology*, **31** (7), 1074-1087. http://dx.doi.org/10.1002/joc.2336

[5] Webster, P.J. and Yang, S., 1992. Monsoon and ENSO: selectively interactive systems. *Quarterly Journal - Royal Meteorological Society*, **118** (507), 877-926. http://dx.doi.org/10.1002/qj.49711850705

[6] Dash, S.K., Kulkarni, M.A., Mohanty, U.C. and Prasad, K., 2009. Changes in the characteristics of rain events in India. *Journal of Geophysical Research: Atmospheres*, **114** (10), art. no. D10109. http://dx.doi.org/10.1029/2008JD010572

[7] Bollasina, M.A., Ming, Y. and Ramaswamy, V., 2011. Anthropogenic aerosols and the weakening of the south asian summer monsoon. *Science*, **334** (6055), 502-505. http://dx.doi.org/10.1126/science.1204994

[8] Saha, A., Ghosh, S., Sahana, A.S., Rao, E.P., 2014. Failure of CMIP5 climate models in simulating post-1950 decreasing trend of Indian monsoon. *Geophysical Research Letters*, **41** (20), 7323-7330. http://dx.doi.org/10.1002 /2014GL061573

[9] Thompson, D. W. J., and J. M. Wallace, 1998: The Arctic Oscillation signature in the wintertime geopotential height and temperature fields. *Geophys. Res. Lett.*, **25**, 1297-1300. http://dx.doi.org/10.1029/98GL00950

[10] Thompson, D. W. J., and J. M. Wallace, 2000: Annular Modes in the Extratropical Circulation. Part I: Month-to-Month Variability. *J. Climate*, **13**, 1000-1016. https://doi.org/10.1175/1520-0442(2000)013<1000:AMITEC>2.0.CO;2

[11] Forsythe, N., Hardy, A.J., Fowler, H.J. Blenkinsop, S., Kilsby, C.G., Archer, D.R. and Hashmi, M.Z., 2015. A detailed cloud fraction climatology of the Upper Indus Basin and its implications for near surface air temperature. *Journal of Climate*, **28** (9), 3537-3556. DOI:10.1175/JCLI-D-14-00505.1

[12] Zhao, Y., Huang, A., Zhou, Y., Huang, D., Yang, Q., Ma, Y., Li, M. and Wei, G., 2014. Impact of the middle and upper tropospheric cooling over central Asia on the summer rainfall in the Tarim Basin, China. *Journal of Climate*, **27** (12), 4721-4732. http://dx.doi.org/10.1175/JCLI-D-13-00456.1

[13] Hewitt, K., 2005. The Karakoram Anomaly? Glacier Expansion and the 'Elevation Effect,' Karakoram Himalaya. *Mountain Research and Development*, **25** (4), 332-340. http://dx.doi.org/10.1659/0276-4741(2005)025[0332:TKAGEA]2.0.CO;2

[14] Fowler, H. J. and Archer, D. R., 2006. Conflicting Signals of Climate Change in the Upper Indus Basin, *J. Climate*, **19** (17), 4276–4292. http://dx.doi.org/10.1175/JCLI3860.1

[15] Sharif, M., Archer, D. R., Fowler, H. J. and Forsythe, N., 2013. Trends in timing and magnitude of flow in the Upper Indus Basin. *Hydrol. Earth Syst. Sci.*, **17** (4), 1503-1516. http://dx.doi.org/10.5194/hess-17-1503-2013

[16] Forsythe, N., Kilsby, C.G., Fowler, H.J. and Archer, D.R., 2012. Assessment of Runoff Sensitivity in the Upper Indus Basin to Interannual Climate Variability and Potential Change Using MODIS Satellite Data Products. *Mountain Research and Development*, **32** (1), 16-29. http://dx.doi.org/10.1659/MRD-JOURNAL-D-11-00027.1

[17] Dee, D.P., Uppala et al, 2011. The ERA-Interim reanalysis: configuration and performance of the data assimilation system. *Q. J. R. Meteorol. Soc*. **137** (656), 553–597. http://dx.doi.org/10.1002/qj.828

[18] Ebita, A. et al, 2011. The Japanese 55-year Reanalysis "JRA-55": An Interim Report. *Scientific Online Letters on the Atmosphere*, **7**, 149-152. http://dx.doi.org/10.2151/sola.2011-038